



**HAL**  
open science

## Ocean acidification causes variable trait-shifts in a coral species

Núria Teixidó, Erik Caroselli, Samir Alliouane, Chiara Ceccarelli, Steeve Comeau, Jean-Pierre Gattuso, Pietro Fici, Fiorenza Micheli, Alice Mirasole, Stephen Monismith, et al.

### ► To cite this version:

Núria Teixidó, Erik Caroselli, Samir Alliouane, Chiara Ceccarelli, Steeve Comeau, et al.. Ocean acidification causes variable trait-shifts in a coral species. *Global Change Biology*, 2020, 26 (12), pp.6813-6830. 10.1111/gcb.15372 . hal-03374987

**HAL Id: hal-03374987**

**<https://hal.science/hal-03374987>**

Submitted on 12 Oct 2021

**HAL** is a multi-disciplinary open access archive for the deposit and dissemination of scientific research documents, whether they are published or not. The documents may come from teaching and research institutions in France or abroad, or from public or private research centers.

L'archive ouverte pluridisciplinaire **HAL**, est destinée au dépôt et à la diffusion de documents scientifiques de niveau recherche, publiés ou non, émanant des établissements d'enseignement et de recherche français ou étrangers, des laboratoires publics ou privés.



## Ocean acidification causes variable trait shifts in a coral species

Journal:	<i>Global Change Biology</i>
Manuscript ID	GCB-20-1585
Wiley - Manuscript type:	Primary Research Articles
Date Submitted by the Author:	24-Jul-2020
Complete List of Authors:	<p>Teixido, Nuria; Stazione Zoologica Anton Dohrn, Villa Dohrn-Benthic Ecology Center; CNRS-UPMC, Laboratoire d'Océanographie de Villefranche</p> <p>Caroselli, Erik; Alma Mater Studiorum - University of Bologna, Department of Biological, Geological, and Environmental Sciences, University of Bologna</p> <p>Alliouane, Samir; CNRS-UPMC, Laboratoire d'Océanographie de Villefranche</p> <p>Ceccarelli, Chiara; Alma Mater Studiorum - University of Bologna, Department of Biological, Geological, and Environmental Sciences</p> <p>Comeau, Steeve; CNRS-UPMC, Laboratoire d'Océanographie de Villefranche</p> <p>Gattuso, Jean-Pierre; CNRS-UPMC, Laboratoire d'Océanographie de Villefranche</p> <p>Fici, Pietro ; Alma Mater Studiorum - University of Bologna, Department of Biological, Geological, and Environmental Sciences</p> <p>Micheli, Fiorenza; Stanford University, Hopkins Marine Station</p> <p>Mirasole, Alice; Stazione Zoologica Anton Dohrn</p> <p>Monismith, Stephen; Stanford University, Department of Civil and Environmental Engineering</p> <p>Munari, Marco; Stazione Zoologica Anton Dohrn, Villa Dohrn-Benthic Ecology Center</p> <p>Palumbi, Stephen; Stanford University, Hopkins Marine Station</p> <p>Sheets, Elisabeth; Stanford University, Hopkins Marine Station</p> <p>Urbini, Lidia; Istituto Nazionale di Oceanografia e Geofisica Sperimentale</p> <p>De Vittor, Cinzia; Istituto Nazionale di Oceanografia e Geofisica Sperimentale</p> <p>Goffredo, Stefano; Alma Mater Studiorum - University of Bologna, Department of Biological, Geological and Environmental Sciences</p> <p>Gambi, Maria Cristina; Stazione Zoologica Anton Dohrn, Villa Dohrn-Benthic Ecology Center</p>
Keywords:	corals, calcification, ocean acidification, variable environments, natural CO <sub>2</sub> vents, acclimatization/adaptation
Abstract:	High pCO <sub>2</sub> habitats and their populations provide an unparalleled opportunity to assess how species may survive under future ocean acidification conditions, and help to reveal the traits that confer tolerance. Here we utilize a unique CO <sub>2</sub> vent system to study the effects

	<p>of exposure to elevated <math>p\text{CO}_2</math> on trait-shifts observed throughout natural populations of <i>Astroides calycularis</i>, an azooxanthellate scleractinian coral endemic to the Mediterranean. Unexpected shifts in skeletal and growth patterns were found. Colonies shifted to a skeletal phenotype characterized by encrusting morphology, smaller size, reduced coenosarc tissue, fewer polyps, and less porous and denser skeletons at low pH. Interestingly, while individual polyps calcified more and extended faster at low pH, whole colonies found at low pH site calcified and extended their skeleton at the same rate as did those at ambient pH sites. Transcriptomic data revealed strong genetic differentiation among local populations of this warm water species whose distribution range is currently expanding northward. We found excess differentiation in the <math>\text{CO}_2</math> vent population for genes central to calcification, including genes for calcium management (calmodulin, calcium-binding proteins), pH regulation (V-type proton ATPase), and inorganic carbon regulation (carbonic anhydrase). Combined, our results demonstrate how coral populations can persist in high <math>p\text{CO}_2</math> environments, making this system a powerful candidate for investigating acclimatization and local adaptation of organisms to global environmental change.</p>

## **Ocean acidification causes variable trait shifts in a coral species**

1

2

3 Nuria Teixidó<sup>1,2\*</sup>, Erik Caroselli<sup>3\*</sup>, Samir Alliouane<sup>2</sup>, Chiara Ceccarelli<sup>3</sup>, Steeve Comeau<sup>2</sup>, Jean-  
4 Pierre Gattuso<sup>2,4</sup>, Pietro Fici<sup>3</sup>, Fiorenza Micheli<sup>5,6</sup>, Alice Mirasole<sup>1</sup>, Stephen G. Monismith<sup>7</sup>,  
5 Marco Munari<sup>1</sup>, Stephen R. Palumbi<sup>5</sup>, Elizabeth Sheets<sup>5</sup>, Lidia Urbini<sup>8</sup>, Cinzia De Vittor<sup>8</sup>,  
6 Stefano Goffredo<sup>3,9\*</sup>, Maria Cristina Gambi<sup>1</sup>

7

8 <sup>1</sup>Stazione Zoologica Anton Dohrn, Ischia Marine Centre, Punta San Pietro 80077, Ischia, Naples,  
9 Italy.

10 <sup>2</sup>Sorbonne Université, CNRS, Laboratoire d'Océanographie de Villefranche, 181 chemin du  
11 Lazaret, 06230 Villefranche-sur-mer, France.

12 <sup>3</sup>Marine Science Group, Department of Biological, Geological, and Environmental Sciences,  
13 University of Bologna, Via Selmi 3, 40126 Bologna, Italy.

14 <sup>4</sup>Institute for Sustainable Development and International Relations, Sciences Po, 27 rue Saint  
15 Guillaume, F-75007 Paris, France

16 <sup>5</sup>Department of Biology, Hopkins Marine Station, Stanford University, Pacific Grove, CA,  
17 93950, USA.

18 <sup>6</sup>Stanford Center for Ocean Solutions, Pacific Grove, CA, 93950, USA.

19 <sup>7</sup>Department of Civil and Environmental Engineering, Stanford University, Stanford, CA, 94305,  
20 USA.

21 <sup>8</sup>Istituto Nazionale di Oceanografia e di Geofisica Sperimentale (OGS), Via A. Piccard 54,  
22 34151, Trieste, Italy.

23 <sup>9</sup>Fano Marine Center, Department of Biological, Geological and Environmental Sciences,

24 University of Bologna, viale Adriatico 1/N, 61032 Fano, Italy

25 \*corresponding author. Email: [nuria.teixido@obs-vlfr.fr](mailto:nuria.teixido@obs-vlfr.fr) ; [erik.caroselli@unibo.it](mailto:erik.caroselli@unibo.it) ;

26 [s.goffredo@unibo.it](mailto:s.goffredo@unibo.it)

27

For Review Only

**28 Abstract**

29 High  $p\text{CO}_2$  habitats and their populations provide an unparalleled opportunity to assess how  
30 species may survive under future ocean acidification conditions, and help to reveal the traits that  
31 confer tolerance. Here we utilize a unique  $\text{CO}_2$  vent system to study the effects of exposure to  
32 elevated  $p\text{CO}_2$  on trait-shifts observed throughout natural populations of *Astroides calycularis*, an  
33 azooxanthellate scleractinian coral endemic to the Mediterranean. Unexpected shifts in skeletal  
34 and growth patterns were found. Colonies shifted to a skeletal phenotype characterized by  
35 encrusting morphology, smaller size, reduced coenosarc tissue, fewer polyps, and less porous and  
36 denser skeletons at low pH. Interestingly, while individual polyps calcified more and extended  
37 faster at low pH, whole colonies found at low pH site calcified and extended their skeleton at the  
38 same rate as did those at ambient pH sites. Transcriptomic data revealed strong genetic  
39 differentiation among local populations of this warm water species whose distribution range is  
40 currently expanding northward. We found excess differentiation in the  $\text{CO}_2$  vent population for  
41 genes central to calcification, including genes for calcium management (calmodulin, calcium-  
42 binding proteins), pH regulation (V-type proton ATPase), and inorganic carbon regulation  
43 (carbonic anhydrase). Combined, our results demonstrate how coral populations can persist in high  
44  $p\text{CO}_2$  environments, making this system a powerful candidate for investigating acclimatization and  
45 local adaptation of organisms to global environmental change.

46

47

## 48 1. INTRODUCTION

49 Understanding the effects of environmental variability and extremes on natural populations and  
50 ecosystems is a key priority as global environmental change intensifies (Bennett, Duarte, Marba,  
51 & Wernberg, 2019; Bozinovic, Calosi, & Spicer, 2011). High local variability in physical and  
52 chemical ocean properties can create extreme climatic environments, where marine species persist  
53 under suboptimal environmental conditions such as highly variable temperatures, marginal  
54 habitats at latitudinal extremes, and acidification at CO<sub>2</sub> vent sites (Camp et al., 2018; Kapsenberg  
55 & Cyronak, 2019; Kroeker et al., 2019). Populations living in these unique settings experience  
56 high environmental variability and can have broad physiological tolerance to environmental  
57 stressors that would prevent survival of conspecifics living in less variable micro-environments  
58 (Bozinovic et al., 2011; Thomas et al., 2018). Two important mechanisms for intraspecific  
59 variation in tolerance to environmental variability and extremes are adjusting life traits through  
60 phenotypic plasticity and local adaptation, and these processes may interact synergistically  
61 (Hoffmann & Sgro, 2011; Savolainen, Lascoux, & Merilä, 2013). Phenotypic plasticity (also  
62 referred to as acclimatization) is the ability of a genotype to produce different morphological and  
63 physiological responses when exposed to different environmental conditions within an organism's  
64 lifespan, resulting in a phenotypic shift that is plastic and often reversible (Savolainen et al., 2013;  
65 Thomas et al., 2018). Adaptation is the result of natural selection on beneficial genotypes in a  
66 population where these changes are heritable and passed on to the next generation (Hoffmann &  
67 Sgro, 2011; Savolainen et al., 2013). Natural extreme environments are potential locations for  
68 climate-adapted populations where, for example, microhabitats experiencing periodic temperature  
69 extremes have shown to generate high-tolerance in some reef-building corals (Palumbi, Barshis,  
70 Traylor-Knowles, & Bay, 2014; Thomas et al., 2018). However, there is still much to learn about

71 the underlying mechanisms of acclimatization and adaptation to climate variability and extremes  
72 by studying populations in naturally variable environments. Such studies are critical for predicting  
73 future biological responses to rapid global environmental change.

74 Insights into species' tolerance to environmental change may be gained by analyzing traits that  
75 directly influence an organism's performance (Mouillot, Graham, Villéger, Mason, & Bellwood,  
76 2013). Shifts in the occurrence of these traits under variable environmental conditions can reflect  
77 patterns of differential survival and growth strategies; for example, different morphological forms  
78 (e.g. massive or encrusting), longevity, size, growth rates, physical defenses and dispersal ability  
79 (Darling, Alvarez-Filip, Oliver, Mcclanahan, & Côté, 2012; Teixidó et al., 2018). These traits  
80 provide relevant information about life strategies that are the result of different evolutionary and  
81 ecological processes and influence, both the fitness of individuals and the viability of natural  
82 populations (Darling et al., 2012; Mouillot et al., 2013; Teixidó et al., 2018). However, we still  
83 know comparatively little about trait-shifts within natural populations and the capacity to adapt to  
84 long-term novel environmental conditions.

85 Natural volcanic CO<sub>2</sub> vents cause local acidification of seawater and are used as a proxy to study  
86 future ocean acidification (Enochs et al., 2015; Fabricius et al., 2011; Hall-Spencer et al., 2008).  
87 Ocean acidification reflects a suite of changes in seawater carbonate chemistry due to the uptake  
88 of excess anthropogenic CO<sub>2</sub> by the ocean, resulting in a decline in the surface ocean pH, carbonate  
89 ion concentration, and saturation state of calcium carbonate minerals (e.g. aragonite), while  
90 increasing the partial pressure of carbon dioxide ( $p\text{CO}_2$ ) and bicarbonate ion concentrations  
91 (Doney, Fabry, Feely, & Kleypas, 2009). Low pH levels in natural CO<sub>2</sub> vents represent future  
92 climatic conditions where, relative to 1870, surface pH is projected to decline by -0.14 to -0.4 pH  
93 units by 2100, under IPCC Representative Concentration Pathways (RCP) RCP 2.6 (low CO<sub>2</sub>



94 emissions) and RCP 8.5 (high CO<sub>2</sub> emissions) (Fabricius et al., 2011; Gattuso et al., 2015;  
95 Goffredo et al., 2014; Teixidó et al., 2018). Although these pH conditions can provide some insight  
96 into future acidification scenarios, they are not perfect proxies. One important assumption to  
97 consider is that variability of seawater pH increases with decreasing means at CO<sub>2</sub> vent systems.  
98 Although variability in pH/*p*CO<sub>2</sub> will increase with dissolved inorganic carbon due to the  
99 thermodynamics of the carbonate system in the future ocean (Takeshita et al., 2015), it is not  
100 possible to disentangle the effects of changes in the mean versus variability in this system. Thus,  
101 the conditions in the pH zones should be considered as pH regimes, with decreases in mean pH  
102 coinciding with increases in variability. Nevertheless, these high *p*CO<sub>2</sub> environments and their  
103 populations provide an unparalleled opportunity to assess how species may survive into future pH  
104 conditions and to reveal if general traits that confer tolerance can be identified.

105 Corals are key marine organisms that are particularly vulnerable to the impacts of climate change  
106 and ocean acidification (Brandl et al., 2019; Gattuso et al., 2015). They create habitats for many  
107 species, enhancing biodiversity, playing fundamental ecological roles and sustaining ecosystem  
108 processes and services such as fisheries, coastal protection and tourism (Brandl et al., 2019;  
109 Gattuso et al., 2015). Ocean acidification may pose a major threat to corals because their growth  
110 relies on the precipitation of calcium carbonate (calcification), a process that is expected to  
111 decrease as seawater acidity increases (Chan & Connolly, 2013). Studies conducted at CO<sub>2</sub> vent  
112 ecosystems on native corals have reported an overall decline in species abundances, decreases in  
113 calcification and skeletal density with increasing acidification (Fabricius et al., 2011; Fantazzini  
114 et al., 2015; Goffredo et al., 2014).

115 Here we utilize a unique CO<sub>2</sub> vent system to investigate the effects of exposure to elevate *p*CO<sub>2</sub>  
116 on trait-shifts on *Astroides calycularis*, an azooxanthellate scleractinian coral endemic to the

117 Mediterranean, that naturally occurs in the acidified environment of a newly discovered CO<sub>2</sub> vent  
118 system in Ischia, Italy. This CO<sub>2</sub> vent system locally acidifies the seawater with gas comprising  
119 92-95% CO<sub>2</sub> (no sulphur, and no temperature anomaly). *A. calycularis* is a long-lived coral (large  
120 colonies may have a life span of several decades), considered a warm-water species with a narrow  
121 temperature tolerance confined to 14°C during winter (Bianchi, 2007; Zibrowius, 1995). *A.*  
122 *calycularis* has low dispersal capacities, and therefore restricted gene flow (Casado-Amezúa,  
123 Goffredo, Templado, & Machordom, 2012). Because *A. calycularis* is a calcifying and long-lived  
124 species with low dispersal capacity, and found throughout the CO<sub>2</sub> vents, it is a great model system  
125 for investigating variation in local climate phenotypic plasticity and adaptation. Previous research  
126 on the effects of ocean acidification on *A. calycularis* has shown contrasting results: a reduction  
127 of net calcification rates was found when colonies growing in ambient pH conditions were  
128 transplanted to a vent system with pH below 7.7 (Prada et al., 2017), while no change in  
129 calcification under acidification was observed in controlled laboratory conditions (Movilla et al.,  
130 2016). We compare populations living near the vent to two reference areas outside the influence  
131 of CO<sub>2</sub> venting to examine the effects of low pH conditions on *A. calycularis* traits, to characterize  
132 the genetic population structure, and to identify differentiation in genes that are central to  
133 calcification. Specifically, we addressed the following questions: i) do populations at the CO<sub>2</sub> vent  
134 and reference sites exhibit significant trait variation?, ii) do these nearby populations display  
135 genetic differentiation?, and iii) does the CO<sub>2</sub> vent population have highly divergent SNP  
136 genotypes from calcium- related loci? To answer these questions, we characterized the physical  
137 and chemical parameters of the study sites and combined *in situ* population demographics, skeletal  
138 characteristics, computed tomography and transcriptomic approaches to assess changes in  
139 population abundance, skeletal properties, age, and genomics of differentiation of *A. calycularis*.

## 140 2. MATERIAL AND METHODS

### 141 2.1 Experimental design and study sites

142 Here we compare natural populations of the scleractinian coral *A. calycularis* at a volcanic CO<sub>2</sub>  
143 vent and two nearby reference sites with ambient pH and no vent activity along the coast of Ischia,  
144 Italy (Figure 1). The CO<sub>2</sub> vent system is located at a 5 m depth inside a semi-submerged cave of  
145 volcanic origin named *Grotta del Mago* (Magician's Cave, 40°42'41.87"N, 13°57'51.06"E,  
146 hereafter Vent system) (Figure 1). The cave (total length of 110 m) consists of a main outer  
147 chamber (10 m wide x 30 m long), connected to an inner chamber by a long narrow passage  
148 (Cinelli et al., 1977). Published studies and personal observations indicated an increase in the CO<sub>2</sub>  
149 vent activity over the last 50 years in the main chamber, with limited vent activity in the 70's  
150 (Cinelli et al., 1977) and 2000's (Dappiano & Gambi, 2004) developing into intense activity from  
151 2014 onwards. The abundance of *A. calycularis* in the cave has increased over time, with a low  
152 and patchy distribution between 1-2 m depth in the main chamber in the 1970's (Cinelli et al.,  
153 1977) to a high and continuous distribution in the 2000's (Dappiano & Gambi, 2004). The present  
154 study was performed in the main chamber of the cave. The reference sites with ambient pH were  
155 chosen following the criteria: i) *A. calycularis* naturally occurred there, ii) they hosted similar  
156 habitats and depths as the CO<sub>2</sub> vent site, and iii) and no venting activity was evident. Two reference  
157 sites were selected: Punta Vico (40°45'32.28"N, 13°52'55.38"E, another semi-submerged cave,  
158 with a main chamber 10 m wide x 30 m long, 5 m maximum depth, hereafter Ambient 1); and  
159 Sant'Angelo (40°41'33.78"N, 13°53'38.88"E, an overhang, also a natural habitat of *A. calycularis*,  
160 located on a natural arch, with an opening of 10 m wide x 10 m height, 10 m maximum depth,  
161 hereafter Ambient 2). Initial investigations of the natural systems and environmental parameters  
162 started in June, 2016. These preliminary environmental data were used to plan subsequent field

163 samplings of the carbonate chemistry associated with the CO<sub>2</sub> vent system and reference sites in  
164 September, 2018 and June, 2019.

## 165 **2.2 The coral**

166 *A. calycularis* (Pallas, 1766) is an azooxanthellate scleractinian colonial coral endemic to the  
167 Mediterranean, characterized by the bright orange color of its coenosarc and polyps (Zibrowius,  
168 1995). It is considered a long-lived species (*e.g* large colonies may have a life span of several  
169 decades) and commonly found in dimly lit, shallow rocky habitats (vertical walls, cave entrances,  
170 overhangs, from the intertidal fringe to 50 m depths) (Zibrowius, 1995). It can be highly abundant  
171 covering more than 90% of local reefs. It has a limited geographic distribution, with a southwestern  
172 distribution in the Mediterranean Sea (Zibrowius, 1995). This coral is considered a warm-water  
173 species with a narrow temperature tolerance confined to 14°C during the winter (Bianchi, 2007).  
174 Fossil records reveal this species lived in the northwestern Mediterranean during part of the  
175 Pleistocene, where climatic fluctuations occurred leading to a reduction of the species (Zibrowius,  
176 1995). Interestingly, observed records north of its known distribution range in Italy and Croatia  
177 suggest that it is currently expanding northward (Bianchi, 2007). Currently, *A. calycularis* is  
178 assessed as vulnerable on the IUCN Red List due to its limited geographic distribution and the  
179 historical and current regression caused by human activities in the littoral zone. *A. calycularis*  
180 broods its larvae and has relatively low dispersal capacity (Casado-Amezúa et al., 2012).

## 181 **2.3 Gas and temperature**

182 Gas samples were collected in 200 ml glass bottles and analyzed using gas chromatography  
183 (Agilent 7890B combined with a Micro GC analyzer-INFICON, held at a constant temperature of  
184 80 °C). The mean composition of the bubbling gas was predominantly CO<sub>2</sub> (92-95%, with  
185 undetectable levels of sulfur gas <0.0002 %) and did not elevate the temperature (see Supporting

186 Note 1, Figure S1), subsequently resulting in water acidification. Vent activity was sampled by  
187 counting the number of vents in randomly placed 1 m<sup>2</sup> quadrats (n= 11) in the main chamber, with  
188 approximately 5 vents m<sup>-2</sup> (mean  $\pm$  SE= 4.9  $\pm$  2.7 vents m<sup>-2</sup>, min= 2 vents m<sup>-2</sup>; maximum = 11  
189 vents m<sup>-2</sup>). Temperature was registered every hour by *in situ* temperature data loggers (Hobo  
190 TidbiT v2, Onset) in the cave and the reference areas and followed ambient seasonal fluctuations,  
191 from 14.7 to 15.2 °C in winter (n=16,754), and from 25.5 to 26.5 °C in summer (n= 19,011) over  
192 a 3-year period from 2016 to 2019 at 2 m depth (Figure S1, Table S1).

#### 193 **2.4 pH<sub>T</sub> time series, pH<sub>T</sub> variability and pH sensor calibration**

194 SeaFET™ Ocean pH sensors (Satlantic) were deployed to quantify variation in pH inside the cave  
195 at 2, 3 and 4 m depth. They were deployed in May-June (before summer) and in September (after  
196 summer) to assess whether differences in water temperature stratification could influence pH  
197 across depths. Dates of deployment were from September 8 to September 24, 2018 and from May  
198 30 to June 18, 2019. Two sensors were deployed in the reference areas during the same period  
199 (Ambient 1 in September, 2018 and Ambient 2 in June, 2019). Before deployment, the SeaFETs  
200 were calibrated with ambient pH water in the aquarium facilities at the Center Villa Dohrn (Ischia,  
201 Italy) (for full details of pH sensor calibration, see Supporting Methods). The mean offset between  
202 calibration samples and calibrated SeaFET pH was  $\pm$  0.002 units, indicating high quality pH  
203 dataset (Figure S2).

#### 204 **2.5 Carbonate Chemistry and Nutrients**

205 Discrete water samples were collected using Niskin bottles at the vent and reference areas with  
206 ambient pH to measure: i) the carbonate system parameters during the pH sensor deployment, and  
207 ii) dissolved inorganic nutrients. Salinity was measured using a CTD (CTD Sea Bird Electronics  
208 SBE 19 Plus Seacat). Samples for total alkalinity (A<sub>T</sub>) were collected using standard operating

209 protocols (for full details, see Supporting Methods). The HCl (0.1 M) titrant solution was  
210 calibrated against certified reference materials distributed by A.G. Dickson (CRM, Batches #153,  
211 #171, and #177). Precision of the  $A_T$  measurements of CRMs was  $< 2.0 \mu\text{mol kg}^{-1}$  from nominal  
212 values. Means were reported as (mean  $\pm$  SD):  $A_T = 2562.41 \pm 7.8 \mu\text{mol kg}^{-1}$ ,  $n = 27$  in September  
213 2018; and  $A_T = 2543.57 \pm 21.78 \mu\text{mol kg}^{-1}$ ,  $n = 21$  in June 2019.  $A_T$  and  $\text{pH}_T$  were used to determine  
214 the remaining carbonate system parameters at *in situ* temperature and depth of each sampling  
215 period in the R package seacarb v3.2.12 (for constant details, see Supporting Methods). Dissolved  
216 inorganic nutrients (nitrite  $\text{NO}_2$ , nitrate  $\text{NO}_3$ , ammonium  $\text{NH}_4^+$ , phosphate  $\text{PO}_4$  and silicate  
217  $\text{Si}(\text{OH})_4$ ) were determined using a colorimetric method (Supporting Methods) (Table S2).

## 218 **2.6 Coral field surveys: cover, population structure and morphology**

219 The *A. calycularis* cover was quantified using 24 photoquadrats (25 x 25 cm) positioned along six  
220 transects at four depths: 1, 2, 3, and 4 m in the three study sites (Vent, A1, A2). Percentage cover  
221 was analyzed with ImageJ image software (National Institutes of Health,  
222 <https://imagej.net/ImageJ>). Size frequency-distribution was calculated at 1 and 3 m depths by  
223 counting the number of polyps of each colony and each colony was then pooled into one of five  
224 size classes (I: 1-5 polyps; II: 6-10 polyps; III: 11-15 polyps; IV: 16-20 polyps; V:  $> 20$  polyps).  
225 These size classes were selected to span the range of colony sizes encountered in the field. We  
226 also assessed necrosis as the percentage of the colony exhibiting dead tissue or denuded skeleton,  
227 from white-grey to unpigmented or denuded skeleton. Finally, visual assessments were used to  
228 classify the colonies into two morphological categories: encrusting (flat growth form) and massive  
229 (extensive vertical and lateral growth). Encrusting colonies extended laterally over the surrounding  
230 substrate, whereas massive presented a greater vertical accretion which resulted in semi-spherical

231 shapes. This categorical criterion allowed us to obtain two simple morphological variables to  
232 capture biologically relevant axes of variation.

## 233 **2.7 Sample collection for presence of coenosarc, skeletal characteristics and growth**

234 Sixty-six colonies of *A. calycularis* were sampled haphazardly for coenosarc, biometric, growth,  
235 and skeletal parameters. Thirty-four colonies were collected at the vent site: 16 colonies were  
236 obtained from the vicinity of the CO<sub>2</sub> vents at 3 m depth (vent system deep, Vd) and 18 colonies  
237 at 1- 2m depth (vent system shallow, Vs). Thirty-two colonies were collected from areas with  
238 ambient pH conditions: 17 colonies in Punta Vico, Ambient 1, 1 – 2 m depth; and 15 colonies in  
239 Sant'Angelo, Ambient 2, 1 -2 m depth. The 66 colonies were photographed and the percentage of  
240 coenosarc (*i.e.*, the living tissue connecting the polyps) was determined. The % of coenosarc was  
241 determined from the edges of the polyp tissue. The % of coenosarc was classified into ten classes  
242 at every 10% interval, from 100% to 0%. Loss of coenosarc in *A. calycularis* may occur mainly  
243 by two mechanisms: 1) loss of tissue due to necrosis (when colony exhibits dead tissue, from  
244 white-grey to unpigmented or denuded skeleton), or 2) the coenosarc is already absent due to  
245 physiological and morphological characteristic of the colonies.

### 246 **2.7.1 Biometric parameters**

247 Coral skeletons were rinsed in a solution of 10% commercial chlorine bleach for 3-4 days to  
248 dissolve polyp tissue, then they were dried at room temperature for 3 days. Colony was defined as  
249 the whole calcareous skeleton, which included the polyps (corallites) and the coenosteum. The  
250 following parameters were measured: colony length ( $L_c$ , major axis of the colony) and colony  
251 width ( $W_c$ , minor axis of the colony); number of polyps in each colony ( $NP_c$ ), corallite length ( $L_p$ ,  
252 maximum axis of the oral disc) and corallite width ( $W_p$ , minimum axis of the oral disc) (for full  
253 details, see Supporting Methods, Figures S3-S4, and Tables S3-S4).

### 254 **2.7.2 Growth and age estimations**

255 The age of each corallite skeleton was determined by counting the growth bands of 49-70 randomly  
256 selected corallites per site, by means of computerized tomography (CT). Growth bands are  
257 distinguished by a high-density band in winter and a low-density band in summer in temperate  
258 corals (see Supporting Methods). The age of all collected corallites was estimated using the von  
259 Bertalanffy's length-age growth function derived from the CT growth bands analysis. Coral  
260 growth is described by three parameters: linear extension rate (linear growth), net calcification rate  
261 (net mass deposited) and bulk skeletal density (mass per volume unit) (Goffredo et al., 2009). The  
262 measurement of all three components is fundamental when assessing the effect of the environment  
263 on coral growth, since none of the three parameters is a perfect predictor for the other two and  
264 each species can respond differently to environmental conditions. Then, the following three coral  
265 growth parameters were calculated for both polyp and colony levels: 1) linear extension rate; 2)  
266 net calcification rate and 3) bulk skeletal density (see below for bulk skeletal density  
267 measurements) (for full details, see Supporting Methods).

### 268 **2.7.3 Skeletal parameters**

269 Skeletal parameters of colonies were calculated by applying the buoyant weight technique through  
270 the density determination kit of the Ohaus Explorer Pro balance ( $\pm 0.0001$  g; for further details,  
271 see Supporting Methods). This method is based on the Archimedes principle applied to a specimen  
272 after full saturation with the same fluid in which it was submerged. The measurements required to  
273 calculate the skeletal parameters were: density of the fluid medium ( $\rho$ ); dry mass (DW), buoyant  
274 weight of the skeleton (BW= weight of the skeleton minus weight of the water displaced by it),  
275 SW (saturated weight of the coral = weight of the skeleton plus weight of the water enclosed in  
276 its). Measurements were repeated three times to get an average for BW and SW. Based on these



277 measurements, the following parameters were calculated:  $V_{\text{MATRIX}}$  (matrix volume = volume of  
278 the skeleton, excluding the volume of its pores);  $V_{\text{PORES}}$  (pore volume=volume of the pores in the  
279 skeleton),  $V_{\text{TOT}}$  (bulk volume = total volume of the skeleton including its pores). Finally, the  
280 skeletal parameters of colonies were calculated: the micro-density (ratio of DW to  $V_{\text{MATRIX}}$ ); the  
281 bulk density (ratio DW to  $V_{\text{TOT}}$ ); and the porosity (ratio  $V_{\text{PORES}}$  to  $V_{\text{TOT}}$ ).

## 282 **2.8 Sample collection for genetics and transcriptome assembly**

283 *A. calycularis* colonies were haphazardly collected between 1- 2 m depth to compare gene flow  
284 among populations at the study sites. Nineteen colonies from the Vent, 14 colonies from Ambient  
285 1 and 8 colonies from Ambient 2 were sampled for genetic analysis. RNA was extracted from a  
286 single polyp of each colony using a RNeasy kit (Qiagen Inc., Valencia, CA, USA) according to  
287 the manufacturer's instructions (for full details, see Supporting Methods). Approximately 1 $\mu$ g of  
288 RNA was used to construct a cDNA library for each sample using the Illumina TruSeq RNA v2  
289 Kit (Illumina, San Diego, CA, USA) (see Supporting Methods).

290 Libraries were sent to the Genomics Core Facility of the Health Sciences Cores at the University  
291 of Utah (Salt Lake City, Utah, USA) and samples were quantified using a Bioanalyzer (Agilent,  
292 Santa Clara, CA, USA) (see Supporting Methods). We assembled the first *de novo* transcriptome  
293 of *A. calycularis* with samples collected from Ischia. The following programs and scripts were run  
294 on Stanford University's Sherlock cluster and all scripts used in this pipeline  
295 ([https://github.com/bethsheets/Astroides\\_transcriptomics](https://github.com/bethsheets/Astroides_transcriptomics)) along with a general guide are available  
296 on GitHub (doi:10.5281/zenodo.2580291). Four population-specific *de novo* assemblies were  
297 generated using three individuals per population for each population in the program Trinity-2.8.4  
298 (see Supporting Methods). Prior trials mapping to available corallimorpharian genomes produced  
299 incomplete assemblies. Therefore, assembled contigs were validated to be included in the

300 assembly by filtering for only metazoan matches found in the combined UniProt's Swiss-Prot and  
301 TrEMBL databases using BLASTX in the BLAST+ toolkit (see Supporting Methods). Matches  
302 were considered significant at values of  $\leq 1 \times 10^{-3}$  and the top hit for each contig was kept for  
303 assembly filtering and annotation. Transcriptome completeness was assessed using BUSCO v3  
304 (see Supporting Methods) against the metazoan (obd9) set. BUSCO analyses revealed that the final  
305 combined transcriptome was 97% complete (949 complete BUSCOs out of 978 searched: 366  
306 complete single-copy, 583 complete and duplicated; 12 fragmented, and 17 missing). For the 41  
307 individuals used for population analyses, the average overall mapping rates for each population  
308 were as follows: Vent-Grotta Mago 79% (range 71.91 - 85.28), Ambient 1- Punta Vico 80% (range  
309 65 – 84.74), Ambient 2- Sant' Angelo- 80.26% (range 71.91 - 85.28). After filtering, we detected  
310 46,784 biallelic SNPs among the vent and two ambient populations.

### 311 **2.8.1 Mapping and SNP detection**

312 For all 41 samples, raw paired- and single-end sequence files were mapped to the *de novo* assembly  
313 using HISAT2 (see Supporting Methods) with the very-sensitive setting. Duplicate reads due to  
314 PCR were removed with Picard tools (<http://broadinstitute.github.io/picard/>) MarkDuplicates  
315 using the lenient validation stringency. Overall mapping rates were compared among populations  
316 to assess whether certain populations were preferentially mapping to the *de novo* assembly.  
317 Transcriptome-derived single nucleotide polymorphisms (SNPs) were called on all individuals  
318 using SAMtools mpileup and BCFtools (for filter settings, see Supporting Methods).

### 319 **2.8.2 Identifying SNP candidates for environmental selection in high CO<sub>2</sub> conditions and** 320 **enrichment analysis**

321 We identified potential outlier SNPs related to the CO<sub>2</sub> vent location. We calculated pairwise Fst  
322 estimates (Vent - Ambient 1, Vent - Ambient 2, Ambient 1 - Ambient 2) per locus using the basic

323 stats function with HIERFSTAT package in R (see Statistical analyses). We used these  
324 estimates to compare the genetic distance for each SNP between the three populations  
325  $[F_{ST}(\text{Vent-A1}) + F_{ST}(\text{Vent-A2})]/F_{ST}(\text{A1-A2})$ . To identify potential outlier SNPs related to  
326 the CO<sub>2</sub> vent location, we compared the genetic distance for each SNP for the population  
327 comparisons including Grotta Mago to the genetic distance between the ambient  
328 populations A1 and A2  $[F_{ST}(\text{Vent-A1}) + F_{ST}(\text{Vent-A2})]/F_{ST}(\text{A1-A2})$ . SNPs with values over  
329 2 showed an excess of genetic differentiation in the CO<sub>2</sub> Vent compared to the other  
330 ambient pH populations. Using the transcriptome assembly annotations, we searched for  
331 enrichment patterns in the contigs holding these candidate SNPs by using their UniProt  
332 identifiers (<https://www.uniprot.org/>) in a Gene Ontology (GO) search  
333 (<http://geneontology.org/>).

## 334 **2.9 Statistical analyses and data visualization**

335 *Environmental data analyses*: Temperature, pH<sub>T</sub>, SeaFET sensor calibration, carbonate chemistry  
336 and figures were performed using the R packages: seacarb v3.2.12 and ggplot2 v3.1.1 (see  
337 Supporting Methods for R package references). Carbonate system parameter figures in the vent  
338 system were created with Ocean Data View software (version 5.1.2, <http://odv.awi.de>). *Biological*  
339 *surveys*: A linear mixed model was used to test for differences in % cover (logit transformation)  
340 as a function of site (fixed factor, 3 levels), depth (fixed factor, 4 levels) and quadrat as a random

341 effect. Chi-square contingency tables were used to compare the size–frequency distributions  
342 among sites, as well as the frequency of encrusting and massive forms. Kolmogorov-Smirnov two-  
343 sample tests were used to determine whether there were significant differences in necrosis between  
344 the CO<sub>2</sub> vent and ambient pH sites. These analyses were computed using lme4 v1.1.21 package  
345 implemented in R. *Skeletal characteristics and growth*: Relationships between biometrical and  
346 skeletal parameters were calculated using the power function model. Pearson’s correlation  
347 coefficients were calculated for the relationships among biometric and skeletal parameters at both  
348 colony and polyp levels. Spearman’s rank correlation coefficient was used to calculate the  
349 significance of the correlations between colony biometric and skeletal parameters and pH<sub>T</sub>.  
350 ANOVA was used to test % cenosarc (with arcsin transformation), mean mass, polyp number,  
351 bulk density, linear extension rate, calcification rate, and porosity of the colonies and mean length  
352 of corallites among sites. We used the non-parametric Kruskal-Wallis test for differences in means  
353 for data that did not meet the assumption for normality and equal variance. Kruskal-Wallis tests  
354 were applied to mean area, length, width, micro-density of colonies, corallite mean age, polyp  
355 linear extension rate, net calcification rate, and length of central and all corallites. These analyses  
356 were computed using IBM SPSS Statistics 12.0 (IBM Corporation). The Von Bertalanffy growth  
357 model and confidence intervals (CI) were estimated through a regression analysis by least squares  
358 procedure using raw data of corallite length and age (measured by computerized tomography) (see  
359 Supporting Methods). These analyses were carried out in the software MATLAB R2012a  
360 (MathWorks, Natick, USA). *Population genetics*: Population genetic analyses of SNPs, Weir and  
361 Cockerham’s pairwise F<sub>ST</sub> estimates among populations, and the heatmap of divergent SNP  
362 genotypes were conducted in the R-based program HIERFSTAT v4.22 and ComplexHeatmap  
363 v2.4.2, respectively.

### 364 3. RESULTS

#### 365 3.1 Carbonate Chemistry Associated with the CO<sub>2</sub> vent system in the *Grotta del Mago*' cave

366 The CO<sub>2</sub> vent system occurs at a 5 m depth inside the main chamber of the cave *Grotta del Mago*  
367 with approximately 5 vents m<sup>-2</sup> (Figure 1) and do not elevate temperature (Table1, Figure S1,  
368 Table S1). The carbonate chemistry derived from discrete water samples and *in situ* monitoring of  
369 seawater pH<sub>T</sub> (pH on the total scale) delineated a pH<sub>T</sub> gradient from 4 m to 2 m depth caused by  
370 the distance from the bubbling of CO<sub>2</sub> gas from the seafloor (92-95% CO<sub>2</sub>, with undetectable levels  
371 of sulfur gas < 0.0002 %, see Supporting Note 1) (Figure 1, Table 1). pH sensors revealed  
372 reductions in mean pH<sub>T</sub> at each depth associated with increased temporal variability in pH<sub>T</sub> (Figure  
373 1, Table 1, Figure S5, Table S5). Mean pH<sub>T</sub> were: 7.65 to 7.88 at 2 m; 7.62 to 7.74 at 3 m, and  
374 7.60 to 7.60 at 4 m, respectively (see Table 1 and Table S5 for detailed pH statistics). At 2 m depth,  
375 14% and 56% of the pH<sub>T</sub> measurements were below 7.8 (projected average global sea surface pH  
376 value for the year 2100 with the high emission scenarios RCP8.5) (Gattuso et al., 2015) in June  
377 and September, respectively (Table S5). The percentage rose to 34% and 61% at 3 m depth, and  
378 55% and 66% at 4 m depth, in June and September, respectively (Table S5). This pattern of depth-  
379 dependent low pH<sub>T</sub> was also manifested as extreme pH events (defined as the pH value of 0.4 units  
380 less than the mean pH for each depth) that increased in number and duration with depth (Table  
381 S6). Mean pH<sub>T</sub> and variability were influenced by temperature stratification in June and September  
382 (Figure 1, Figures S5-S6). This is because during periods of stratification, and hence reduced  
383 vertical mixing (Turner, 1973), the input of CO<sub>2</sub> is likely to be primarily confined to the lower part  
384 of the water column, leading to lower pH values near bed than when the water column is well  
385 mixed. The mean temperature difference between 2 m and 4 m in June was 0.25 °C, whereas the  
386 mean temperature difference was only 0.02 °C in September (Figure S6). In September, reductions

387 in seawater  $pH_T$  were driven by increased dissolved inorganic carbon concentrations ( $C_T$ ) and  
388 higher  $pCO_2$  concentrations at relatively constant total alkalinities ( $A_T$ ) and temperatures across  
389 depths (Table 1, Figure S5). Mean  $pCO_2$  ranged from  $2905 \pm 1664 \mu\text{atm}$  at 2 m, to  $3146 \pm 1928$   
390  $\mu\text{atm}$  at 3 m, to  $3192 \pm 1806 \mu\text{atm}$  at 4m depth, and aragonite saturation state ( $\Omega_a$ ) ranged from  
391  $1.10 \pm 0.4$  at 2m, to  $1.05 \pm 0.4$  at 3 m, and to  $1.02 \pm 0.4$  at 4m depth (Table 1). In contrast, in June,  
392 the vent site was characterized by an increase in temperature along the water column (from  $\sim 18.5$   
393  $^{\circ}\text{C}$  to  $\sim 25^{\circ}\text{C}$ ), which created greater difference across the three depths in terms of  $pH_T$  and  
394 associated carbonate chemistry parameters, particularly for the  $pCO_2$  concentrations (from  $1531 \pm$   
395  $627 \mu\text{atm}$  at 2 m, to  $2082 \pm 1502 \mu\text{atm}$  at 3 m, and  $2812 \pm 2310 \mu\text{atm}$  at 4 m depth) and  $\Omega_a$  (from  
396  $1.44 \pm 0.27$  at 2 m, to  $1.23 \pm 0.35$  at 3 m, to  $1.05 \pm 0.42$  at 4 m depth) (Table 1, Figure S5). At the  
397 two ambient pH sites, the mean  $pH_T$  ranged from 7.97 to 8.05 units,  $pCO_2$  from  $322 \pm 34$  to  $586 \pm$   
398  $76 \mu\text{atm}$ , and  $\Omega_a$  from  $3.54 \pm 0.23$  to  $3.86 \pm 0.23$  (Table 1).

### 399 **3.2 Cover, population structure, and morphology of *A. calycularis***

400 The  $CO_2$  vent population was characterized by small colonies (90% colonies had up to 10 polyps)  
401 and no large colonies of more than 20 polyps (class V) with massive morphology were found  
402 (Figure 2, Figure S7). Larger colonies (*i.e.*  $> 16$  polyps, size classes IV and V) were only found in  
403 the two reference areas (percentage of larger size classes ranged from 13% in A1 to 16 % in A2),  
404 which differed significantly among the  $CO_2$  vent site ( $\chi^2 = 91.9$ ,  $df = 8$ ,  $p < 0.0001$ ). Additionally,  
405 necrosis was significantly higher at the  $CO_2$  vent site ( $13 \pm 4\%$ ) than the reference areas (both  
406  $< 0.5\%$ ,  $D = 0.56$ ,  $p < 0.0001$ ). *A. calycularis*' cover at the  $CO_2$  vent site decreased from 50% at 1 m  
407 depth, to 30% at 2m, 9% at 3 m, and 1% at 4m depth, as seawater  $pH_T$  also declined (Figure S7).  
408 This decline in coral cover was also observed in Ambient 1 (also a cave, from 69% at 1 m to 14%

409 at 3 m) but not in Ambient 2 (overhang, from 72% at 1 m to 62% at 3 m;  $F= 14.1$ ,  $df=11,55$ ;  
410  $p<0.001$ ) (Figure S7).

### 411 **3.3 Coenosarc, skeletal parameters and growth**

412 Percentage of coenosarc (the living tissue connecting the polyps) significantly decreased between  
413 ambient pH sites (87 and 70%) and the CO<sub>2</sub> vent (28 and 14%) (Figure 2,  $p<0.0001$ ). Mean colony  
414 area decreased by ~ 80 - 71% and mean polyp number by ~ 27 - 18% at the Vent deep compared  
415 to ambient pH sites ( $p < 0.001$ ) (Figure 3A). The skeletal parameters that characterize the  
416 architecture of colonies showed different patterns in relation to pH (Figure 3A-B, Figures S8-S9).  
417 Bulk density (ratio dry mass to bulk volume) and micro-density (ratio of dry mass to matrix  
418 volume) increased at low pH, while porosity (ratio pore volume to bulk volume; see Methods)  
419 decreased at low pH ( $p < 0.001$ ; Figure 3A-B). Colonies at the CO<sub>2</sub> vent deep presented higher  
420 bulk density (~ + 27 %) and micro-density (~ + 7 %) and lower porosity (~ -28 %) compared to  
421 colonies from the ambient pH sites ( $p < 0.001$ ) (Figure 3A-B, Figure S9).

422 Growth parameters of *A. calycularis* differed significantly between the CO<sub>2</sub> vent site and ambient  
423 pH sites (Figure 3B, Figure 4, Figure S10, Table S7). Mean polyp growth rate decreased  
424 exponentially with age at all sites (Figure S10). Young individuals (1–3 years old) grew relatively  
425 rapidly ( $> 2 \text{ mm yr}^{-1}$ ), but, as they aged, their skeletal growth rate decreased ( $< 1.3 \text{ mm yr}^{-1}$  at 8–  
426 10 years old) (Figure 4, Tables S7-S8). A trend toward higher linear extension and net calcification  
427 rate was observed at low pH at the polyp level (Figure 3B, Table S7). Polyp net calcification rate  
428 ranged from  $3.95 \text{ mg mm}^{-2} \text{ yr}^{-1}$  at Vent deep, to  $3.04 \text{ mg mm}^{-2} \text{ yr}^{-1}$  at Vent shallow, to  $2.39 \text{ mg}$   
429  $\text{mm}^{-2}\text{yr}^{-1}$  and  $2.06 \text{ mg mm}^{-2} \text{ yr}^{-1}$  at ambient pH sites (Table S7). This indicates that net calcification  
430 rates increased approximately by 48%-93% from the more acidified (Vent deep) to the less  
431 acidified (Vent shallow) to the non-acidified (ambient pH) locations at polyp level. Linear

432 extension and net calcification rates at colony level were homogenous in ambient pH and acidified  
433 conditions (Figure 3B, Table S7).

### 434 **3.4 Transcriptome assembly and population genomics**

435 The *A. calycularis* transcriptome composed of 12 colonies contained 113,351 contigs with an N50  
436 of 2,285 (range 501 – 38,179). Based on 46,784 SNPs in 41 individuals, PCA analysis revealed  
437 strong clustering by population (Figure 5). The vent population in Grotta Mago was most distinct  
438 along PCA axis 1, but overlapped with Ambient1 (PV) along axis 2. Pairwise  $F_{ST}$  measurements  
439 also support strong population structure within each of the three locations: CO<sub>2</sub> vent (Grotta Mago)  
440 – Ambient 1 (Punta Vico) = 0.034, CO<sub>2</sub> vent (Grotta Mago) – Ambient 2 (Sant'Angelo) = 0.026,  
441 Ambient 1 (Punta Vico) – Ambient 2 (Sant'Angelo) = 0.024. SNPs with values over 2 show an  
442 excess of genetic differentiation in GM compared to the other populations. There were 334 loci  
443 with an excess  $F_{ST}$  ratio of 10 or more, out of 2246 loci in our data set with known molecular  
444 function. An analysis of the 402 unique molecular function Gene Ontology (GO) terms associated  
445 with these loci showed there to be three significant enrichment classes (Table S9): calcium ion  
446 binding (12 loci,  $p_{adj} = 7 \times 10^{-23}$ ), catalytic activity (4 loci,  $p_{adj} = 2 \times 10^{-9}$ ), and  
447 oxidoreductase action (12 loci,  $p_{adj} = 0.05$ ).

448 Calcium ion loci include calmodulin, calcineurin, calnexin, calcium-binding proteins in the  
449 sarcoplasmic reticulum, and a set of two poorly characterized proteins with calcium binding motifs  
450 (Contigs 3436 and 7780). These proteins are EF-hand calcium-binding protein and C-type lectin  
451 calcium-binding in a hmmer database search (<https://www.ebi.ac.uk/Tools/hmmer/>). Because



452 calcium ion control is particularly central to calcification in scleractinians, we examined the 77  
453 SNPs from the thirteen calcium-related loci for patterns across populations (Figure 6). As  
454 expected, the Grotta Mago population had highly divergent SNP genotypes at these loci (average  
455 minor allele frequency difference of 0.24), but these genes also showed a strong degree of  
456 linkage among SNP genotypes within a single gene often across 1000s of base pairs (Figure 6).  
457 Such multi-SNP haplotypes are rare in our data set yet occur in 8 of 10 high excess, calcium ion  
458 loci with multiple SNPs.

459 Given the strong differences in calcium management suggested by excess differentiation  
460 of calcium ion genes in Grotta Mago, we queried our transcriptome SNP data base for  
461 other genes potentially involved in calcification. In corals, calcification occurs in the  
462 calicoblastic space through a combination of high calcium concentration and high pH (reviewed  
463 in Drake et al., 2020). High pH is achieved through proton transport by specific calcium/proton  
464 pumps, including the plasma membrane calcium ATPase (PMCA). There were no PMCA  
465 polymorphisms in our data set, but the V-type ATPase proton pump (contig DN1551, SNPs 1701-  
466 1805) showed six of seven SNPs with strong differentiation in Grotta Mago (excess 0.03 -28.8,  
467 average 11.4, Figure 6). Minor allele frequencies differed by about a factor of 2 in Grotta Mago  
468 compared to the other locations, and SNPs show strong linkage.

469 In addition to genes involved in calcium and pH regulation, we explored possible adaptation in  
470 genes managing intracellular carbonate chemistry. Coral calcification depends on the delivery of  
471 CO<sub>2</sub> to the calicoblastic layer where it is converted to carbonate ions (Cohen & McConnaughey,

472 2003). In *A. calycularis*, a plethora of carbonate related genes showed high differentiation and high  
473 linkage in Grotta Mago, including carboxylases and transporters, but the most interesting is a  
474 carbonic anhydrase (Contig 15508, 5 of 12 SNPs with excess  $F_{st}$  above 10, average=10.3).  
475 Carbonic anhydrases convert highly diffusive  $CO_2$  into charged carbonate ions, localizing them in  
476 the calicoblastic layer and regulating calcification (Chen, Gagnon, & Adkins, 2018), though they  
477 also play a role in pH regulation of non-calcifying coral cells (Bertucci et al., 2013).

#### 478 4. DISCUSSION

479 This study contributes to increasing our understanding of how coral populations persist under  
480 naturally high  $pCO_2$  environments – and therefore how they might cope under future ocean  
481 acidification scenarios – and links trait-shifts with local variation in environmental parameters found  
482 in this new  $CO_2$  vent system. Our results expand upon previous research on populations of corals  
483 exposed to naturally elevated  $pCO_2$  (Crook, Cohen, Rebolledo-Vieyra, Hernandez, & Paytan, 2013;  
484 Enochs et al., 2015; Fabricius et al., 2011; Fantazzini et al., 2015), demonstrating unexpected shifts  
485 in patterns of skeleton and growth of the azooxanthellate coral *A. calycularis*. Specifically,  
486 colonies shift to a skeletal phenotype characterized by encrusting morphology, smaller size,  
487 reduced coenosarc tissue, fewer polyps, and less porous and denser skeletons at low pH. However,  
488 while individual polyps calcified more (greater net calcification rates), calcification rate of whole  
489 colonies were similar across sites. The resulting colony skeletons showed equal linear extension  
490 at low and ambient pH conditions, while their polyp skeletons extended faster in acidified  
491 conditions (Figure 7). Transcriptomic data revealed strong genetic differentiation among local  
492 populations of this low-dispersal species. We found excess differentiation in the Grotta Mago  
493 population for genes central to calcification, including genes for calcium management

494 (calmodulin, calcium-binding proteins), pH regulation (V-type proton ATPase), and carbonate  
495 localization (carbonic anhydrase).

496

497 *Environmental variability in the CO<sub>2</sub> vent system*

498 The vent system exhibits high temporal variability in seawater pH due to varying CO<sub>2</sub> venting  
499 intensity from the seabed, mixing due to variations in stratification, and fundamental  
500 thermodynamics processes fundamental to the carbonate system (Takeshita et al., 2015). The  
501 carbonate chemistry and *in situ* monitoring of seawater pH delineated a pH gradient (from 4 to 2  
502 m depth) caused by the distance from the venting. This acidification gradient is important for the  
503 colonies exposed to more (deep) or less (shallow) acidified conditions, as reflected by the  
504 biological response of *Astroides*. The conditions in these zones are comparable with IPCC  
505 projections for near future acidification scenarios (RCP2.6 and RCP8.5), which project a decrease  
506 in surface pH from  $-0.14$  to  $-0.4$  pH units by 2100 relative to 1870 (Gattuso et al., 2015). pH and  
507 its variability found in this study are comparable with the range of natural variation observed in  
508 other CO<sub>2</sub> vent systems, with fluctuations of 0.6, 0.7 and 0.5 pH units in coral reefs (Agostini et  
509 al., 2018), temperate reefs in Panarea (Prada et al., 2017) and in other CO<sub>2</sub> vents in Ischia (Teixidó  
510 et al., 2018), respectively. Likewise, Hofmann et al. (2011) reported pH fluctuations between 0.024  
511 to 1.430 pH units, in which pH measurements were taken from different locations, ranging from  
512 polar to tropical, and open-ocean to coastal areas. Interestingly, as mean pH was reduced, its  
513 variability and the percentage of pH<sub>T</sub> measurements registered below 7.8 units increased, when  
514 seawater was uniformly warm. In contrast, in June when the water column was stratified, pH and  
515 its variability near the bottom was similar to what was observed in September whereas, farther

516 from the bottom, pH was higher and less variable. These results indicate that seawater stratification  
517 may play a key role in controlling the temporal and depth patterns of pH/pCO<sub>2</sub>.

518

### 519 *Shifts in coral skeleton, growth, and coenosarc*

520 Each scleractinian coral species may adopt different growth strategies in response to ocean  
521 acidification. For example, investing calcification resources in bulk skeletal density by sacrificing  
522 the rate of linear extension has been observed in *Orbicella annularis* (Carricart-Gavinet, 2007). In  
523 contrast, investing calcification resources in linear extension rate at the expense of bulk density  
524 has been reported for some *Porites* (Lough & Barnes, 2000) and Dendrophyllidae species  
525 (Goffredo et al., 2009). Both strategies may imply different ecological trade-offs for the coral:  
526 investing in a denser skeleton results in greater resistance to mechanical stress, while increasing  
527 linear extension rate may be advantageous for space competition and earlier sexual maturity  
528 (Goffredo et al., 2009). Unexpectedly, *A. calycularis* revealed unusual patterns in the calcification  
529 response to ocean acidification, such as higher bulk skeletal density and lower porosity while  
530 maintaining colony linear extension rates and net calcification. This response is different to what  
531 was previously shown in solitary corals (e.g. *Balanophyllia europaea*) growing in natural low pH  
532 conditions, where a decrease of net calcification resulted from preserving linear extension (to reach  
533 the polyp size of sexual maturity) at the expenses of lower bulk density (e.g. increased in skeletal  
534 porosity resulting in more fragile skeletons) (Fantazzini et al., 2015). Tambutté et al.(2015) found  
535 the same response of decreasing calcification and bulk skeletal density while linear extension of  
536 skeleton remained unchanged in the tropical coral *Stylophora pistillata* subjected to low pH  
537 conditions in laboratory. Mollica et al. (2018) modelled the skeletal growth to changes in seawater  
538 chemistry and predicted declines in *Porites* skeletal density but no linear extension across global

539 reefs, reflecting the large variability in the response of coral calcification to ocean acidification.  
540 The authors suggested that under low-pH conditions, the increase in linear extension reflects the  
541 elongation of calcium carbonate crystals at the site of calcification, while the increase in skeletal  
542 density reflects the lateral thickening of calcified elements of coral skeleton (Mollica et al., 2018).  
543 The unusual response of *A. calycularis* to acidification may reflect an overall maintenance of  
544 energetic resources allocated to calcification at the level of the colonies, which extended at the  
545 same rate but were composed by fewer polyps, thus partitioning the available energy for  
546 calcification among fewer polyps (Swain et al., 2018). We can therefore reasonably assume that  
547 nutrients levels, and potentially the zooplankton, did not differ among study sites (Supporting  
548 Material Table S2). As a result, a single polyp would have more energetic resources available for  
549 calcification than in ambient pH conditions, as indicated by their greater skeletal growth  
550 parameters. This particular response may be possible in *A. calycularis* due to its colonial nature.  
551 We hypothesize that in order to maintain the calcification rate at the colony level, colonies tend to  
552 decrease their number of polyps, but in turn, their few polyps extend their skeleton faster to reach  
553 the size of sexual maturity. No asexual division (fragmentation) has been observed over 5 years in  
554 *A. calycularis* in the three study sites, suggesting that this strategy of reproduction is not common.  
555 *A. calycularis* exhibited at the vent site a morphological shift to encrusting and smaller colonies,  
556 with less porous, and potentially more robust corallite skeletal architecture.  
557 While individuals from the vents were composed of corallites with higher skeletal density, this  
558 was less evident at the colony level. While skeletal integrity was not strictly quantified,  
559 observations at the vent site showed that the colonies were more fragile and lost their integrity  
560 more readily, suggesting that the section of the skeleton located between the polyps (coenosteum)  
561 was either less calcified and/or more prone to dissolution. This could be the result of thinner or

562 absent coenosarc (the tissue covering the coenosteum) found in the colonies at the CO<sub>2</sub> vent.  
563 Contrasting responses between skeletal parts that either are or are not protected by living tissues  
564 has already been reported for corals (Hennige et al., 2015; Ries, 2011; Rodolfo-Metalpa et al.,  
565 2011). This loss of coenosarc could indicate the beginning of a further shift from colonial forms  
566 towards solitary polyps to ensure survivorship, as has occurred throughout the history of  
567 scleractinian coral evolution and in laboratory conditions (Fine & Tchernov, 2007; Kvitt et al.,  
568 2015). Interestingly, it was recently shown that following a heatwave and a bleaching event, the  
569 Mediterranean coral *Cladocora caespitosa* suffered from apparent mortality but its tissues actually  
570 retracted inside the individual corallites before rejuvenescence occurred a few years later (Kersting  
571 & Linares, 2019). Here, we hypothesize that a similar, but less extreme phenomenon occurred with  
572 the corals reducing their coenosarc in response to low pH. A reduction in tissue thickness can have  
573 implications for calcification because the precipitation of calcium carbonate occurs in the  
574 calcifying fluid that is a medium semi-isolated from the external seawater by the overlying coral  
575 tissues. To promote calcification, corals have the ability to upregulate pH and C<sub>T</sub> (dissolved  
576 inorganic carbon) concentrations in the calcifying fluid (Comeau, Cornwall, & McCulloch, 2017),  
577 a capacity that is reduced under ocean acidification (McCulloch, Falter, Trotter, & Montagna,  
578 2012). Here reduced calcification between the polyps was likely due to a reduction of coral ability  
579 to maintain optimal carbonate chemistry conditions in the calcifying fluid between the polyps. This  
580 could have been the result of natural spatial heterogeneity sensitivity of colonies to acidification  
581 (Holcomb et al., 2014). In addition to reduced calcification, thinning or disappearing of the tissues  
582 likely led to local dissolution because exposed skeletons are more prone to dissolution (Ries,  
583 2011). As a result of reduced calcification and dissolution of the coenosteum, colonies at the vent  
584 site were weaker and smaller despite heavily calcified corallites.

585

586 *Genomics of differentiation of corals at the CO<sub>2</sub> vent system*

587 Our results show strong genetic differentiation of all three *A. calycularis* populations ( $F_{ST}$   
588 averaging 0.024 – 0.034), with over 5000 SNPs showing  $F_{ST}>0.10$ . A previous genetic study of *A.*  
589 *calycularis* using microsatellites also found significant genetic differentiation at km-scale  
590 distances, likely a reflection of this species limited dispersal capabilities (Casado-Amezúa et al.,  
591 2012). These data showed strong linkage among SNPs across 1000s of bp within genes and strong  
592 linkage across different genes. These patterns could be generated by selective sweeps acting on a  
593 small number of founder colonies, but because linkage among genes and SNPs occurs among  
594 ambient pH (Ambient 1 and Ambient 2) individuals as well as Vent corals. These linkages were  
595 probably not due to recent selection at the CO<sub>2</sub> vent site alone but reflect the underlying  
596 architecture of adaptation. *A. calycularis* is a warm-water coral whose distribution range is  
597 currently expanding northward (Bianchi, 2007), where Ischia belongs to the north-east margin of  
598 the confirmed distribution. As a result, it is also likely that selection is acting at the Ambient 1 and  
599 2 sites compared to more southerly populations. Disentangling the ways in which selection at high  
600 CO<sub>2</sub> locations combines with selection at higher temperatures may be particularly important in  
601 future ocean conditions. The matrix of genetically distinct populations of *A. calycularis*  
602 experiencing a variety of selection regimes for heat and CO<sub>2</sub> may be a powerful setting for this  
603 future work.

604 The most highly differentiated genes in the vent site population, Grotta Mago, are  
605 annotated for calcium regulation, proton pumping, and inorganic carbon regulation. It is  
606 possible that they are differentiated in Grotta Mago for reasons other than selection on

607 calcification in the presence of high CO<sub>2</sub>. However, the strong shift in alleles at these loci  
608 and the linkage among those differentiated SNPs provides a strong set of hypotheses for  
609 the way selection might act to favor coral calcification at low pH.

610 Two loci of calmodulin were highly differentiated in Grotta Mago, with linked SNPs in our  
611 data set. Calcium transporter genes are thought to be important in delivering calcium to  
612 the calciblastic space (Allemand, Tambutté, Zoccola, & Tambutté, 2011). Though the  
613 precise mechanism is not known, calmodulin along with calbindin and calreticulin are  
614 hypothesized to play a role in managing calcium levels and can be sensitive to pH  
615 (Allemand et al., 2011). For example, Kaniewska et al. (2012) showed 8-fold down  
616 regulation of calmodulin in a CO<sub>2</sub>-treated reef building coral. An increase in calcium at the  
617 site of calcification has been shown as a mean to alleviate the negative effect of low pH in some  
618 corals (Decarlo, Comeau, Cornwall, & McCulloch, 2018). Our data also showed excess  
619 differentiation in genes that depend on calcium concentrations for their function, such as  
620 calineurin, calnexin and the sarcoplasmic reticulum histidine-rich calcium-binding protein,  
621 which are thought to play a role in calcium homeostasis.



622 Intracellular and vacuolar H<sup>+</sup> concentrations are central to coral calcification by controlling  
623 pH of the calcifying fluid and the calciblastic and gastrodermal cells. The V-type ATPase  
624 proton pump is localized in the symbiosomes of corals that contain intracellular symbionts  
625 (Tresguerres, 2016), but is also highly expressed in non-symbiotic gastroderm of  
626 symbiont-free tips of quickly calcifying corals, suggesting a role in calcification in the  
627 absence of symbionts (Perez, 2015). In particular, the protein VHA (V-type proton  
628 ATPase) is differentially regulated in corals exposed to low pH, being downregulated  
629 more than four fold in experiments on the reef building coral *Acropora millepora*  
630 (Kaniewska et al., 2012). The population of *A. calicularis* in Grotta Mago showed strong  
631 differentiation at 6 SNPs across a 100 bp region of this gene.

632 CO<sub>2</sub> diffuses very quickly through cells, and is hard to localize in cell regions that need it  
633 for photosynthesis or calcification. Carbonic anhydrase catalyzes the reaction to convert  
634 CO<sub>2</sub> to carbonate ions that diffuse much less quickly. As a consequence, carbonic  
635 anhydrase is central to calcification in many marine species. In fact, Zebral et al. (2019)  
636 suggest use of it as a biomarker to monitor effects of acidification. In corals, carbonic  
637 anhydrase is thought to favor carbonate ion concentration in the calciblastic space and

638 in symbiosomes through conversion of CO<sub>2</sub> (Chen et al., 2018; Zoccola et al., 2016).  
639 However, low-pH experiments on a deep water coral (*Lophelia pertusa*) did not find strong  
640 shifts in carbonic anhydrase activity, nor did an examination of carbonic anhydrase in  
641 polychaete worms from the Ischia CO<sub>2</sub> vents (Del Pasqua, Gambi, Caricato, Lionetto, &  
642 Giangrande, 2019). Experiments on reef building corals have shown mixed results  
643 (Kurihara, Takahashi, Reyes-Bermudez, & Hidaka, 2018). We found strong differentiation  
644 of one carbonic anhydrase locus in Grotta Mago. An average shift in minor allele  
645 frequency from 0.14 to 0.50 in six linked SNPs may signal differential activity of this gene  
646 in some functionally important way. These SNPs appear to be downstream of the  
647 carbonic anhydrase coding region and if they play a role it may be as allele-specific  
648 regulators of expression. These allele differences may be a good tool to understand the  
649 role of carbonic anhydrase in reaction to high CO<sub>2</sub>.

650 In conclusion, our study demonstrates that the natural population of the azooxanthellate coral *A.*  
651 *calycularis* living near the CO<sub>2</sub> vent system shows variable responses in terms of skeleton and  
652 growth patterns that result in a shift in phenotypic and ecological traits. We have shown that these  
653 variable responses at the polyp and colony level allow this coral to cope with low and variable pH  
654 in the long term by re-allocating energy investments between individual and colony growth as well

655 as mineralogical characteristics. Transcriptomic data revealed strong genetic differentiation among  
656 local populations with several candidate loci and linkage blocks under selection. In addition, we  
657 found excess differentiation in the CO<sub>2</sub> vent population for genes central to calcification, including  
658 genes for calcium management (calmodulin, calcium-binding proteins), pH regulation (V-type  
659 proton ATPase), and inorganic carbon regulation (carbonic anhydrase). These patterns highlight  
660 both the CO<sub>2</sub> vents as well as the fringes of this species' expansion as potential drivers of  
661 adaptation.

662

For Review Only

663 **REFERENCES**

- 664 Agostini, S., Harvey, B. P., Wada, S., Kon, K., Milazzo, M., Inaba, K., & Hall-Spencer, J. M.  
665 (2018). Ocean acidification drives community shifts towards simplified non-calcified habitats  
666 in a subtropical – temperate transition zone. *Scientific Reports*, 8, 11354.  
667 <https://doi.org/10.1038/s41598-018-29251-7>
- 668 Allemand, D., Tambutté, É., Zoccola, D., & Tambutté, S. (2011). Coral calcification, cells to  
669 reefs. In Z. Dubinsky & N. Stambler (Eds.), *Coral Reefs: An Ecosystem in Transition* (pp. 1–  
670 552). Springer. <https://doi.org/10.1007/978-94-007-0114-4>
- 671 Bennett, S., Duarte, C. M., Marba, N., & Wernberg, T. (2019). Integrating within-species  
672 variation in thermal physiology into climate change ecology. *Philosophical Transactions of the*  
673 *Royal Society B*, 374, 20180550.
- 674 Bertucci, A., Moya, A., Tambutté, S., Allemand, D., Supuran, C. T., & Zoccola, D. (2013).  
675 Carbonic anhydrases in anthozoan corals - A review. *Bioorganic and Medicinal Chemistry*,  
676 21(6), 1437–1450. <https://doi.org/10.1016/j.bmc.2012.10.024>
- 677 Bianchi, C. N. (2007). Biodiversity issues for the forthcoming tropical Mediterranean Sea.  
678 *Hydrobiologia*, 580, 7–21. <https://doi.org/10.1007/s10750-006-0469-5>
- 679 Bozinovic, F., Calosi, P., & Spicer, J. I. (2011). Physiological correlates of geographic range in  
680 animals. *Annual Review of Ecology, Evolution, and Systematics*, 42, 155–179.  
681 <https://doi.org/10.1146/annurev-ecolsys-102710-145055>
- 682 Brandl, S. J., Rasher, D. B., Côté, I. M., Casey, J. M., Darling, E. S., Lefcheck, J. S., & Duffy, J.  
683 E. (2019). Coral reef ecosystem functioning: eight core processes and the role of biodiversity.  
684 *Frontiers in Ecology and the Environment*, 17, 445–454. <https://doi.org/10.1002/fee.2088>

- 685 Camp, E. F., Schoepf, V., Mumby, P. J., Hardtke, L. A., Rodolfo-Metalpa, R., Smith, D. J., &  
686 Suggett, D. J. (2018). The future of coral reefs subject to rapid climate change: lessons from  
687 natural extreme environments. *Frontiers in Marine Science*, 5, 4.  
688 <https://doi.org/10.3389/fmars.2018.00004>
- 689 Carricart-Gavinet, J. P. (2007). Annual density banding in massive coral skeletons: result of  
690 growth strategies to inhabit reefs with high microborers' activity? *Marine Biology*, 153, 1–5.
- 691 Casado-Amezúa, P., Goffredo, S., Templado, J., & Machordom, A. (2012). Genetic assessment  
692 of population structure and connectivity in the threatened Mediterranean coral *Astroides*  
693 *calycularis* (Scleractinia, Dendrophylliidae) at different spatial scales. *Molecular Ecology*, 21,  
694 3671–3685. <https://doi.org/10.1111/j.1365-294X.2012.05655.x>
- 695 Chan, N. C. S., & Connolly, S. R. (2013). Sensitivity of coral calcification to ocean acidification:  
696 a meta-analysis. *Global Change Biology*, 19(1), 282–290.  
697 <https://doi.org/doi:10.1111/gcb.12011>
- 698 Chen, S., Gagnon, A. C., & Adkins, J. F. (2018). Carbonic anhydrase, coral calcification and a  
699 new model of stable isotope vital effects. *Geochimica et Cosmochimica Acta*, 236, 179–197.  
700 <https://doi.org/10.1016/j.gca.2018.02.032>
- 701 Cinelli, F., Fresi, E., Mazzella, L., Pansini, M., Pronzato, R., & Svoboda, A. (1977). Distribution  
702 of benthic phyto- and zoocoenoses along a light gradient in a superficial marine cave. In B. F.  
703 Keegan, P. O. O'Ceidig, & P. J. Boaden (Eds.), *Biology of Benthic organisms* (pp. 173–183).  
704 Pergamon Press, Oxford.
- 705 Cohen, A. L., & McConnaughey, T. A. (2003). Geochemical Perspectives on Coral  
706 Mineralization. In P. M. Dove, S. Weiner, & J. J. DeYoreo (Eds.), *Biom mineralization* (Vol. 54,

- 707 pp. 151–187). The Mineralogical Society of America, Washington, DC.
- 708 <https://doi.org/10.2113/0540151>
- 709 Comeau, S., Cornwall, C. E., & McCulloch, M. T. (2017). Decoupling between the response of  
710 coral calcifying fluid pH and calcification to ocean acidification. *Scientific Reports*, *7*, 7573.  
711 <https://doi.org/10.1038/s41598-017-08003-z>
- 712 Crook, E. D., Cohen, A. L., Rebolledo-Vieyra, M., Hernandez, L., & Paytan, A. (2013). Reduced  
713 calcification and lack of acclimatization by coral colonies growing in areas of persistent natural  
714 acidification. *Proceedings of the National Academy of Sciences of the United States of*  
715 *America*, *110*(27), 11044–11049. <https://doi.org/10.1073/pnas.1301589110>
- 716 Dappiano, M., & Gambi, M. C. (2004). New data on occurrence of thermophile Scleractinia  
717 (Cnidaria, Anthozoa) in the Phlaegrean Island (Ischia, Procida, Vivara, Gulf of Naples), with  
718 special attention to *Astroides calycularis*. *Biogeographia – The Journal of Integrative*  
719 *Biogeography*, *25*, 1–15. <https://doi.org/10.21426/B6110042>
- 720 Darling, E. S., Alvarez-Filip, L., Oliver, T. A., McClanahan, T. R., & Côté, I. M. (2012).  
721 Evaluating life-history strategies of reef corals from species traits. *Ecology Letters*, *15*(12),  
722 1378–1386. <https://doi.org/10.1111/j.1461-0248.2012.01861.x>
- 723 Decarlo, T. M., Comeau, S., Cornwall, C. E., & McCulloch, M. T. (2018). Coral resistance to  
724 ocean acidification linked to increased calcium at the site of calcification. *Proceedings of the*  
725 *Royal Society B: Biological Sciences*, *285*(1878), 20180564.  
726 <https://doi.org/10.1098/rspb.2018.0564>
- 727 Del Pasqua, M., Gambi, M. C., Caricato, R., Lionetto, M. G., & Giangrande, A. (2019). Effects  
728 of short-term and long-term exposure to ocean acidification on carbonic anhydrase activity and

- 729 morphometric characteristics in the invasive polychaete *Branchiomma boholense* (Annelida:  
730 Sabellidae): A case-study from a CO<sub>2</sub> vent system. *Marine Environmental Research*, 144, 203–  
731 212. <https://doi.org/10.1016/j.marenvres.2019.01.011>
- 732 Doney, S. C., Fabry, V. J., Feely, R. A., & Kleypas, J. A. (2009). Ocean Acidification: The Other  
733 CO<sub>2</sub> Problem. *Annual Review of Marine Science*, 1(1), 169–192.  
734 <https://doi.org/10.1146/annurev.marine.010908.163834>
- 735 Drake, J. L., Mass, T., Stolarski, J., Von Euw, S., van de Schootbrugge, B., & Falkowski, P. G.  
736 (2020). How corals made rocks through the ages. *Global Change Biology*, 26(1), 31–53.  
737 <https://doi.org/10.1111/gcb.14912>
- 738 Enochs, I. C., Manzello, D. P., Donham, E. M., Kolodziej, G., Okano, R., Johnston, L., ... Price,  
739 N. N. (2015). Shift from coral to macroalgae dominance on a volcanically acidified reef.  
740 *Nature Climate Change*, 5, 1083–1088. <https://doi.org/10.1038/nclimate2758>
- 741 Fabricius, K. E., Langdon, C., Uthicke, S., Humphrey, C., Noonan, S., De 'ath, G., ... Lough, J.  
742 M. (2011). Losers and winners in coral reefs acclimatized to elevated carbon dioxide  
743 concentrations. *Nature Climate Change*, 1(6), 165–169.  
744 <https://doi.org/10.1038/NCLIMATE1122>
- 745 Fantazzini, P., Mengoli, S., Pasquini, L., Bortolotti, V., Brizi, L., Mariani, M., ... Goffredo, S.  
746 (2015). Gains and losses of coral skeletal porosity changes with ocean acidification  
747 acclimation. *Nature Communications*, 6, 7785. <https://doi.org/10.1038/ncomms8785>
- 748 Fine, M., & Tchernov, D. (2007). Scleractinian coral species survive and recover from  
749 decalcification. *Science*, 315(5820), 1811. <https://doi.org/10.1126/science.1137094>

- 750 Gattuso, J.-P., Magnan, A., Bille, R., Cheung, W. W. L., Howes, E. L., Joos, F., ... Turley, C.  
751 (2015). Contrasting futures for ocean and society from different anthropogenic CO<sub>2</sub> emissions  
752 scenarios. *Science*, *349*, aac4722. <https://doi.org/10.1126/science.aac4722>
- 753 Goffredo, S., Caroselli, E., Mattioli, G., Pignotti, E., Dubinsky, Z., & Zaccanti, F. (2009).  
754 Inferred level of calcification decreases along an increasing temperature gradient in a  
755 Mediterranean endemic coral. *Limnology and Oceanography*, *54*(3), 930–937.
- 756 Goffredo, S., Prada, F., Caroselli, E., Capaccioni, B., Zaccanti, F., Pasquini, L., ... Falini, G.  
757 (2014). Biomineralization control related to population density under ocean acidification.  
758 *Nature Climate Change*, *4*(7), 593–597. <https://doi.org/10.1038/NCLIMATE2241>
- 759 Hall-Spencer, J. M., Rodolfo-Metalpa, R., Martin, S., Ransome, E., Fine, M., Turner, S. M., ...  
760 Buia, M. C. (2008). Volcanic carbon dioxide vents show ecosystem effects of ocean  
761 acidification. *Nature*, *454*(7200), 96–99. <https://doi.org/10.1038/nature07051>
- 762 Hennige, S. J., Wicks, L. C., Kamenos, N. A., Perna, G., Findlay, H. S., & Roberts, J. M. (2015).  
763 Hidden impacts of ocean acidification to live and dead coral framework. *Proceeding Royal*  
764 *Society B*, *282*, 20150990. <https://doi.org/http://dx.doi.org/10.1098/rspb.2015.0990>
- 765 Hoffmann, A. A., & Sgro, C. M. (2011). Climate change and evolutionary adaptation. *Nature*,  
766 *470*, 479–485. <https://doi.org/10.1038/nature09670>
- 767 Hofmann, G. E., Smith, J. E., Johnson, K. S., Send, U., Levin, L. A., Micheli, F., ... Martz, T. R.  
768 (2011). High-frequency dynamics of ocean pH: A multi-ecosystem comparison. *PLoS ONE*,  
769 *6*(12), e28983. <https://doi.org/10.1371/journal.pone.0028983>
- 770 Holcomb, M., Venn, A. A., Tambutté, E., Tambutté, S., Allemand, D., Trotter, J., & McCulloch,



- 771 M. (2014). Coral calcifying fluid pH dictates response to ocean acidification. *Scientific*  
772 *Reports*, 4, 5207. <https://doi.org/10.1038/srep05207>
- 773 Kaniewska, P., Campbell, P. R., Kline, D. I., Rodriguez-Lanetty, M., Miller, D. J., Dove, S., &  
774 Hoegh-Guldberg, O. (2012). Major cellular and physiological impacts of ocean acidification on  
775 a reef building coral. *PLoS ONE*, 7(4), e34659. <https://doi.org/10.1371/journal.pone.0034659>
- 776 Kapsenberg, L., & Cyronak, T. (2019). Ocean acidification refugia in variable environments.  
777 *Global Change Biology*, 00, 1–14. <https://doi.org/10.1111/gcb.14730>
- 778 Kersting, D. K., & Linares, C. (2019). Living evidence of a fossil survival strategy raises hope  
779 for warming-affected corals. *Science Advances*, 5, eaax2950.
- 780 Kroeker, K. J., Bell, L. E., Donham, E. M., Hoshijima, U., Lummis, S., Toy, J. A., & Norton, E.  
781 W. (2019). Ecological change in dynamic environments: Accounting for temporal  
782 environmental variability in studies of ocean change biology, 00, 1–14.  
783 <https://doi.org/10.1111/gcb.14868>
- 784 Kurihara, H., Takahashi, A., Reyes-Bermudez, A., & Hidaka, M. (2018). Intraspecific variation  
785 in the response of the scleractinian coral *Acropora digitifera* to ocean acidification. *Marine*  
786 *Biology*, 165(2), 38. <https://doi.org/10.1007/s00227-018-3295-1>
- 787 Kvitt, H., Kramarsky-Winter, E., Maor-Landaw, K., Zandbank, K., Kushmaro, A., Rosenfeld,  
788 H., ... Tchernov, D. (2015). Breakdown of coral colonial form under reduced pH conditions is  
789 initiated in polyps and mediated through apoptosis. *Proceedings of the National Academy of*  
790 *Sciences of the United States of America*, 112(7), 2082–2086.  
791 <https://doi.org/10.1073/pnas.1419621112>

- 792 Lough, J. M., & Barnes, D. J. (2000). Environmental controls on growth of the massive coral  
793 Porites. *Journal of Experimental Marine Biology and Ecology*, 245, 225–243.
- 794 McCulloch, M., Falter, J., Trotter, J., & Montagna, P. (2012). Coral resilience to ocean  
795 acidification and global warming through pH up-regulation. *Nature Climate Change*, 2(8),  
796 623–627. <https://doi.org/10.1038/nclimate1473>
- 797 Mollica, N. R., Guo, W., Cohen, A. L., Huang, K. F., Foster, G. L., Donald, H. K., & Solow, A.  
798 R. (2018). Ocean acidification affects coral growth by reducing skeletal density. *Proceedings*  
799 *of the National Academy of Sciences of the United States of America*, 115(8), 1754–1759.  
800 <https://doi.org/10.1073/pnas.1712806115>
- 801 Mouillot, D., Graham, N. A. J., Villéger, S., Mason, N. W. H., & Bellwood, D. R. (2013). A  
802 functional approach reveals community responses to disturbances. *Trends in Ecology and*  
803 *Evolution*, 28(3), 167–177. <https://doi.org/10.1016/j.tree.2012.10.004>
- 804 Movilla, J., Calvo, E., Coma, R., Serrano, E., López-Sanz, À., & Pelejero, C. (2016). Annual  
805 response of two Mediterranean azooxanthellate temperate corals to low-pH and  
806 high-temperature conditions. *Marine Biology*, 163, 135. [https://doi.org/10.1007/s00227-016-](https://doi.org/10.1007/s00227-016-2908-9)  
807 2908-9
- 808 Palumbi, S. R., Barshis, D. J., Traylor-Knowles, N., & Bay, R. A. (2014). Mechanisms of reef  
809 coral resistance to future climate change. *Science*, 344, 895–898.  
810 <https://doi.org/10.1126/science.1251336>
- 811 Perez, S. O. (2015). Characterization of sodium potassium -ATPase and vacuolar proton -  
812 ATPase in three coral species from two different clades. Thesis/dissertation. University of  
813 California San Diego. Retrieved from <https://escholarship.org/uc/item/0xp4r2hb>

- 814 Prada, F., Caroselli, E., Mengoli, S., Brizi, L., Fantazzini, P., Capaccioni, B., ... Goffredo, S.  
815 (2017). Ocean warming and acidification synergistically increase coral mortality. *Scientific*  
816 *Reports*, 7, 40842. <https://doi.org/10.1038/srep40842>
- 817 Ries, J. (2011). Acid ocean cover up. *Nature Climate Change*, 1, 294–295.
- 818 Ries, J. B. (2011). A physicochemical framework for interpreting the biological calcification  
819 response to CO<sub>2</sub> -induced ocean acidification. *Geochimica et Cosmochimica Acta*, 75(14),  
820 4053–4064. <https://doi.org/10.1016/j.gca.2011.04.025>
- 821 Rodolfo-Metalpa, R., Houlbrèque, F., Tambutté, É., Boisson, F., Baggini, C., Patti, F. P., ...  
822 Hall-Spencer, J. (2011). Coral and mollusc resistance to ocean acidification adversely affected  
823 by warming. *Nature Climate Change*, 1(9), 1–5. <https://doi.org/10.1038/nclimate1200>
- 824 Savolainen, O., Lascoux, M., & Merilä, J. (2013). Ecological genomics of local adaptation.  
825 *Nature Reviews Genetics*, 14(11), 807–820. <https://doi.org/10.1038/nrg3522>
- 826 Swain, T. D., Bold, E. C., Osborn, P. C., Baird, A. H., Westneat, M. W., Backman, V., &  
827 Marcelino, L. A. (2018). Physiological integration of coral colonies is correlated with  
828 bleaching resistance. *Marine Ecology Progress Series*, 586, 1–10.  
829 <https://doi.org/10.3354/meps12445>
- 830 Takeshita, Y., Frieder, C. A., Martz, T. R., Ballard, J. R., Feely, R. A., Kram, S., ... Smith, J. E.  
831 (2015). Including high frequency variability in coastal ocean acidification projections.  
832 *Biogeosciences* (Vol. 12). <https://doi.org/10.5194/bgd-12-7125-2015>
- 833 Tambutté, E., Venn, A. A., Holcomb, M., Segonds, N., Techer, N., Zoccola, D., ... Tambutté, S.  
834 (2015). Morphological plasticity of the coral skeleton under CO<sub>2</sub>-driven seawater acidification.

- 835 *Nature Communications*, 6(7368), 1–9. <https://doi.org/10.1038/ncomms8368>
- 836 Teixidó, N., Gambi, M. C., Parravicini, V., Kroeker, K., Micheli, F., Villéger, S., & Ballesteros,  
837 E. (2018). Functional biodiversity loss along natural CO<sub>2</sub> gradients. *Nature Communications*,  
838 9, 5149. <https://doi.org/10.1038/s41467-018-07592-1>
- 839 Thomas, L., Rose, N. H., Bay, R. A., López, E. H., Morikawa, M. K., Ruiz-Jones, L., & Palumbi,  
840 S. R. (2018). Mechanisms of thermal tolerance in reef-building corals across a fine-grained  
841 environmental mosaic: lessons from Ofu, American Samoa. *Frontiers in Marine Science*, 4,  
842 434. <https://doi.org/10.3389/fmars.2017.00434>
- 843 Tresguerres, M. (2016). Novel and potential physiological roles of vacuolar-type H<sup>+</sup>-ATPase in  
844 marine organisms. *Journal of Experimental Biology*, 219(14), 2088–2097.  
845 <https://doi.org/10.1242/jeb.128389>
- 846 Turner, J. S. (1973). *Buoyancy Effects in Fluids*. Cambridge University Press.
- 847 Zebral, Y. D., Da Silva Fonseca, J., Marques, J. A., & Bianchini, A. (2019). Carbonic anhydrase  
848 as a biomarker of global and local impacts: Insights from calcifying animals. *International*  
849 *Journal of Molecular Sciences*, 20(12), 1–16. <https://doi.org/10.3390/ijms20123092>
- 850 Zibrowius, H. (1995). The “southern” *Astroides calycularis* in the Pleistocene of the northern  
851 Mediterranean—An indicator of climatic changes (Cnidaria, Scleractinia). *Geobios*, 28, 9–16.
- 852 Zoccola, D., Innocenti, A., Bertucci, A., Tambutté, E., Supuran, C. T., & Tambutté, S. (2016).  
853 Coral carbonic anhydrases: Regulation by ocean acidification. *Marine Drugs*, 14, 109.  
854 <https://doi.org/10.3390/md14060109>
- 855

## 856 ACKNOWLEDGEMENTS

857 We thank P. Sorvino (ANS Diving, Ischia), A. Passaretti and E. Di Meglio for their field assistance.  
858 We also thank S. Durante (Rizzoli Orthopaedic Institute of Bologna) for assistance in performing  
859 computerized tomography scans and F. Italiano (National Institute of Geophysics and  
860 Volcanology) for the gas data. N.T. thanks M. Khamla for assistance in Figure 7 and E. Ferrer for  
861 English grammar reviewing. **Funding:** This research was supported by the Total Foundation  
862 (High-CO<sub>2</sub> Seas grant, Grant No. BIO-2016-081-4), the French National Research Agency  
863 (4Oceans-MOPGA grant, ANR-17-MPGA-0001), and the ALMA IDEA (STRAMICRO grant,  
864 University of Bologna). N.T. was supported by a Maire Curie-Cofund (FP7-PEOPLE-Marie Curie  
865 Bandiera-Cofund, GA No. 600407) and by a Marie Skłodowska-Curie Global Fellowship under  
866 the European Union's Horizon 2020 research and innovation programme (H2020- MSCA- IF-  
867 2015, GA No. 702628).

## 868 DATA AVAILABILITY STATEMENT

869 RNASeq FASTQ files for all 41 samples sequenced in this study were deposited in the NCBI Short  
870 Read Archive (SRA) under BioProject PRJNA643775 (Accession numbers SRR12135922 -  
871 SRR12135962), <https://dataview.ncbi.nlm.nih.gov/object/PRJNA643775?reviewer=5j14na61906tr4dne0bvg9kbhq>.  
872 The de novo transcriptome assembly generated in this study and used for mapping the samples has  
873 been deposited in the NCBI Transcriptome Shotgun Assembly (TSA) database at  
874 DDBJ/ENA/GenBank under accession number GIRZ01000000  
875 (<https://www.ncbi.nlm.nih.gov/nucleotide/GIRZ00000000>). The version described in this paper  
876 is the first version, GIRZ01000000. The bioinformatics scripts used for assembly, mapping, and  
877 SNP-calling are available on Github at DOI: 10.5281/zenodo.3934433.

878

**879 AUTHOR CONTRIBUTIONS**

880 N.T., E.C., S.P., E.S., S.G., M.C.G designed the study. N.T., E.C., S.A., S.C., F.M., A.M., M.M.,  
881 S.P., E.S., L.U., C.d.V, M.C.G were involved with fieldwork. N.T., S.A., J.P.G., A.M., S.G.M.,  
882 L.U., C.d.V. analyzed the environmental data; E.C., C.C., P.F., S.G. analyzed the skeletal data; E.  
883 S., S. P., and N.T analyzed the genomic data. N.T. drafted the initial manuscript and all authors  
884 contributed discussion, writing and interpretation.

**885 COMPETING INTERESTS**

886 The authors declare that they have no competing interests.

**887 ETHICAL STATEMENT**

888 All work undertaken in this study complied with current laws of Italy and United States of America  
889 for collecting and importing/exporting coral specimens. Cites permits IT/EX/2018/MCE/00170,  
890 IT/EX/2017/MCE/00214, IT/EX/2017/MCE/00325.

## 892 FIGURES AND TABLES

893

894

895

896

897

898

899

900

901

902

903

904

905

906

907

908

909

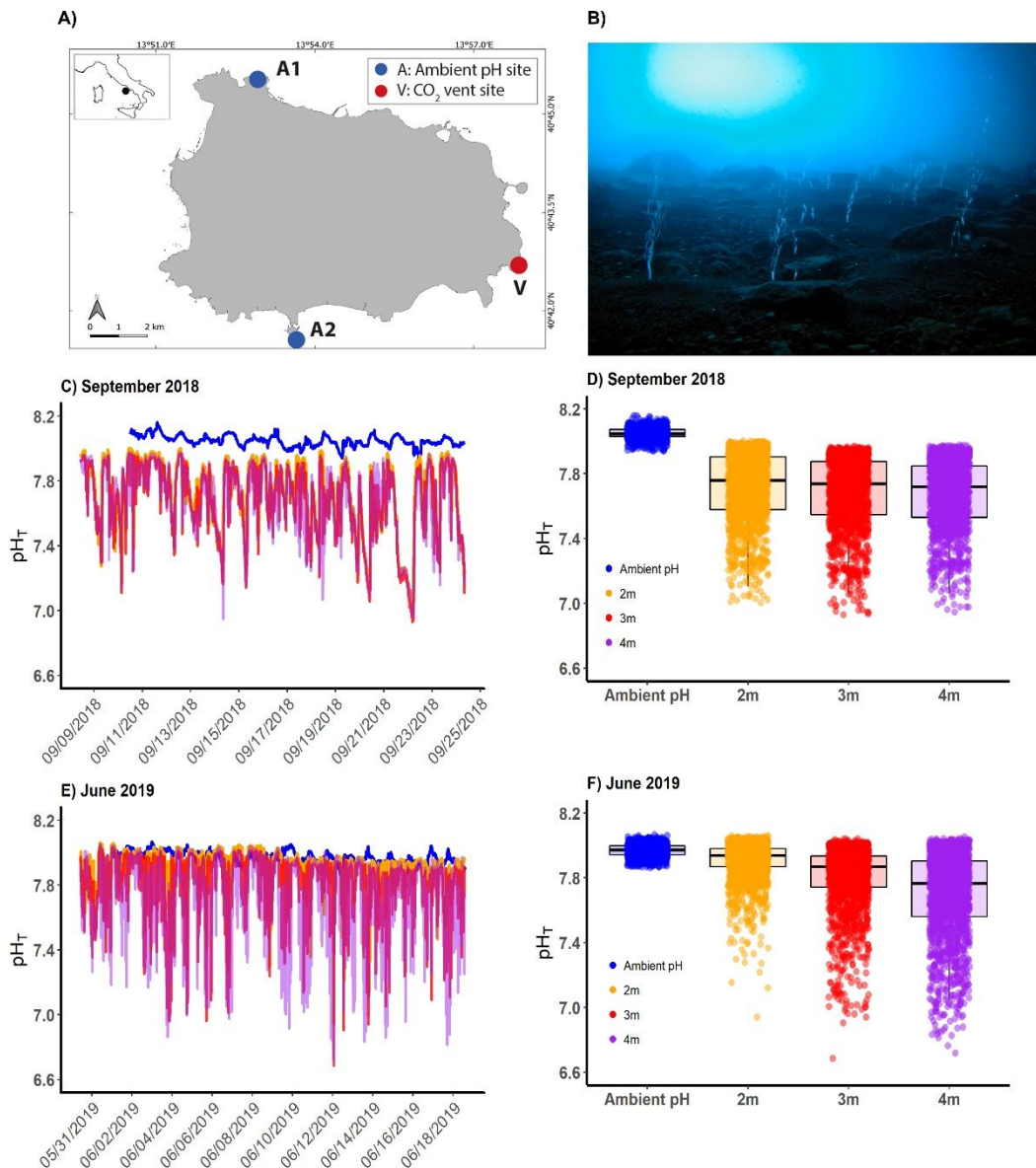
910

911

912

913

914



915 **FIGURE 1. New CO<sub>2</sub> vent system and pH time series and variability.** A) Map showing the

916 location of the study sites along the coast of Ischia Island, Italy. V refers to the CO<sub>2</sub> vent system

917 named *Grotta del Mago*: A1 (Ambient 1, Punta Vico) and A2 (Ambient 2, Sant'Angelo) are off-

918 vent reference sites with ambient pH. B) The underwater volcanic vents occur in a semi-submerged

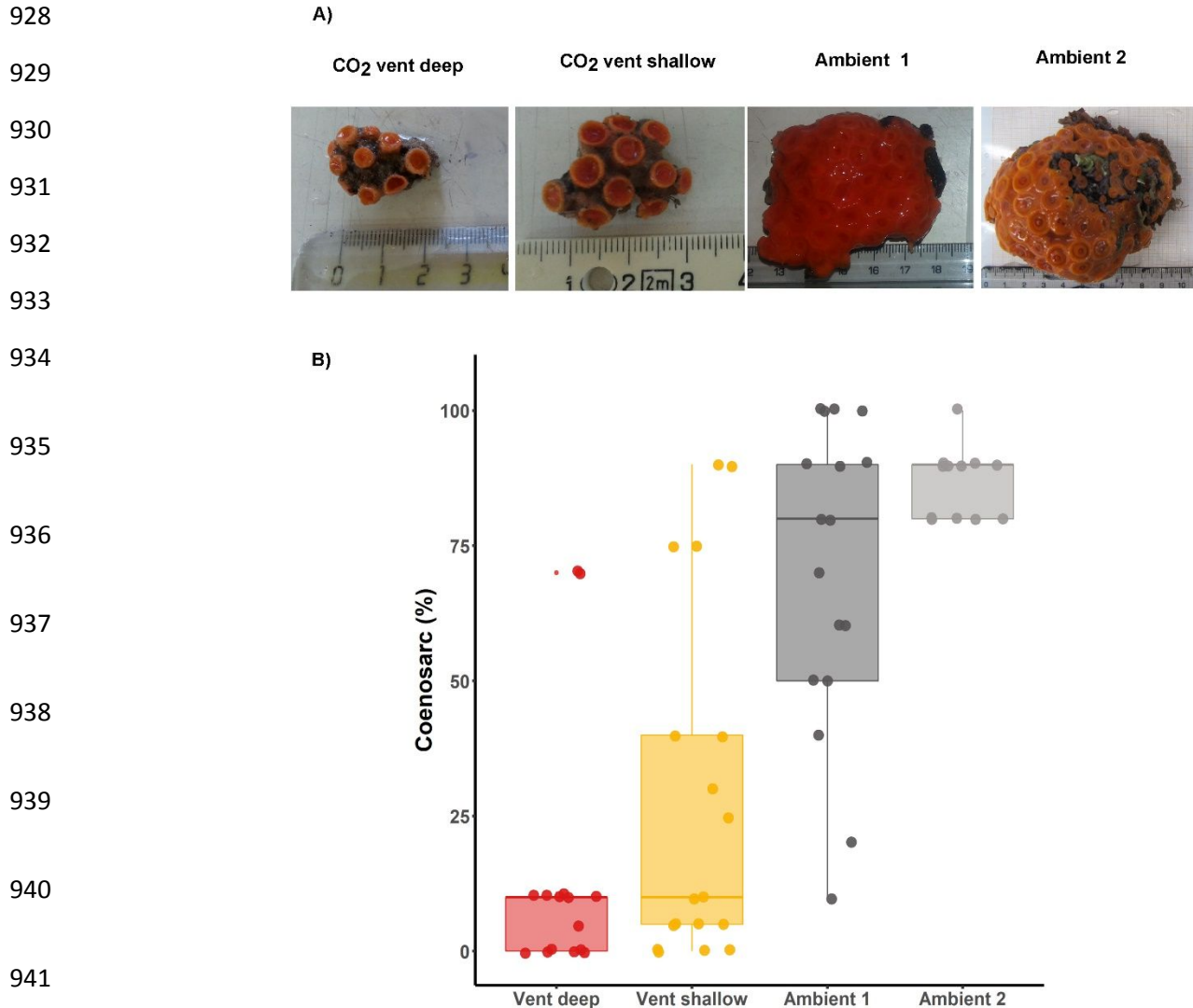
919 cave at 5 m depth, release continuously gaseous emissions (92-95% CO<sub>2</sub>, no sulfur), and do not

920 elevate temperature (Supporting Note 1, Figure S1, Tables S1, S5). C, E) Time series and D, F)  
921 and  $\text{pH}_T$  (total scale) variability at the  $\text{CO}_2$  vent site at 2 m (orange), 3 m (red), and 4 m (violet)  
922 depth and at reference sites at 2 m with ambient pH (blue). Dates of  $\text{pH}_T$  series: from September 8  
923 to September 24, 2018 ( $n= 1530$  for each depth at the  $\text{CO}_2$  vent site and  $n= 1331$  for the ambient  
924 pH site 1), and from May 30 to June 18, 2019 ( $n= 1840$  for each depth at the  $\text{CO}_2$  vent site and  $n=$   
925  $1691$  for the ambient pH site 2). Measurements were taken every 15 minutes using SeaFETs  
926 sensors.

927

For Review Only

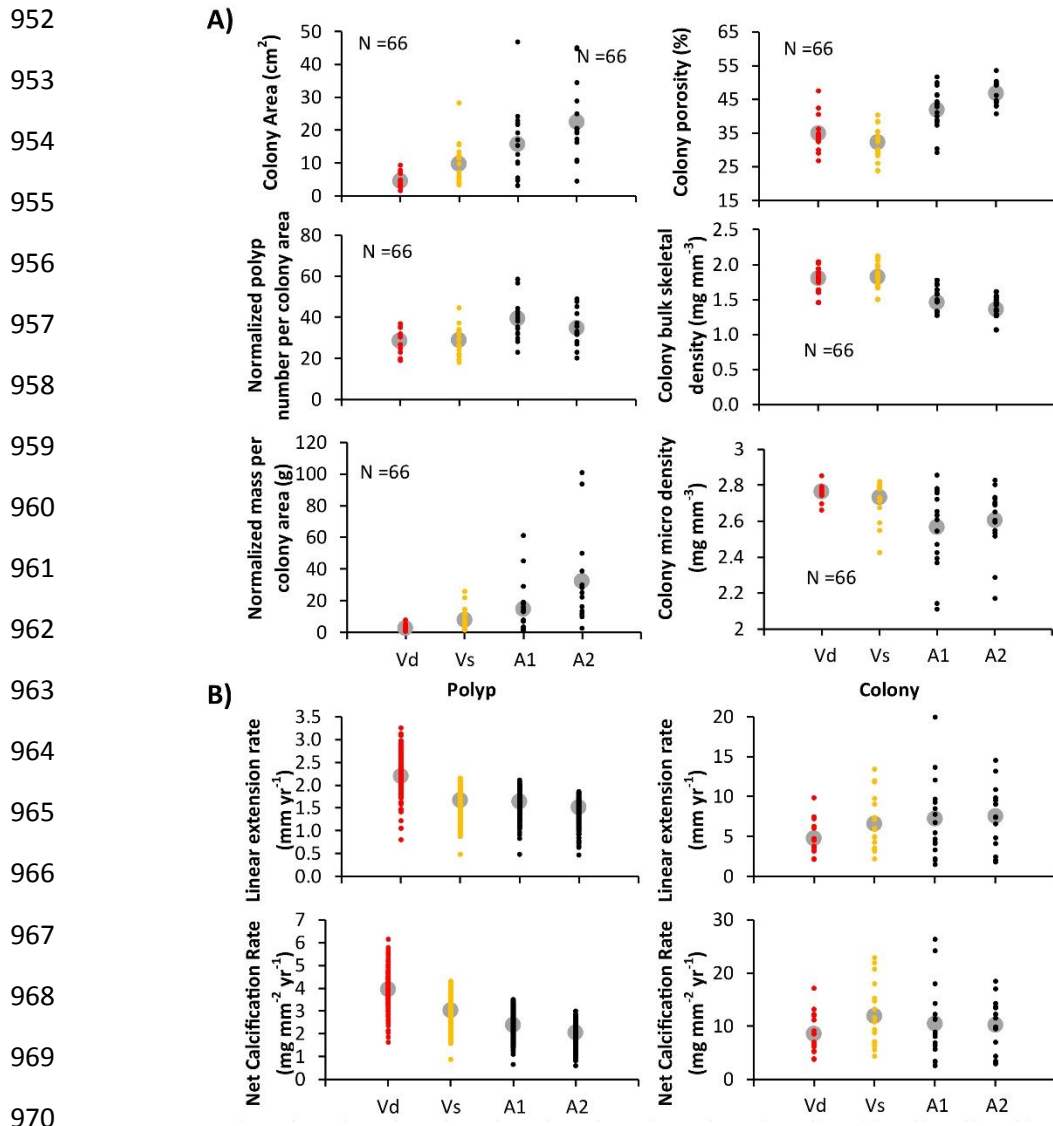




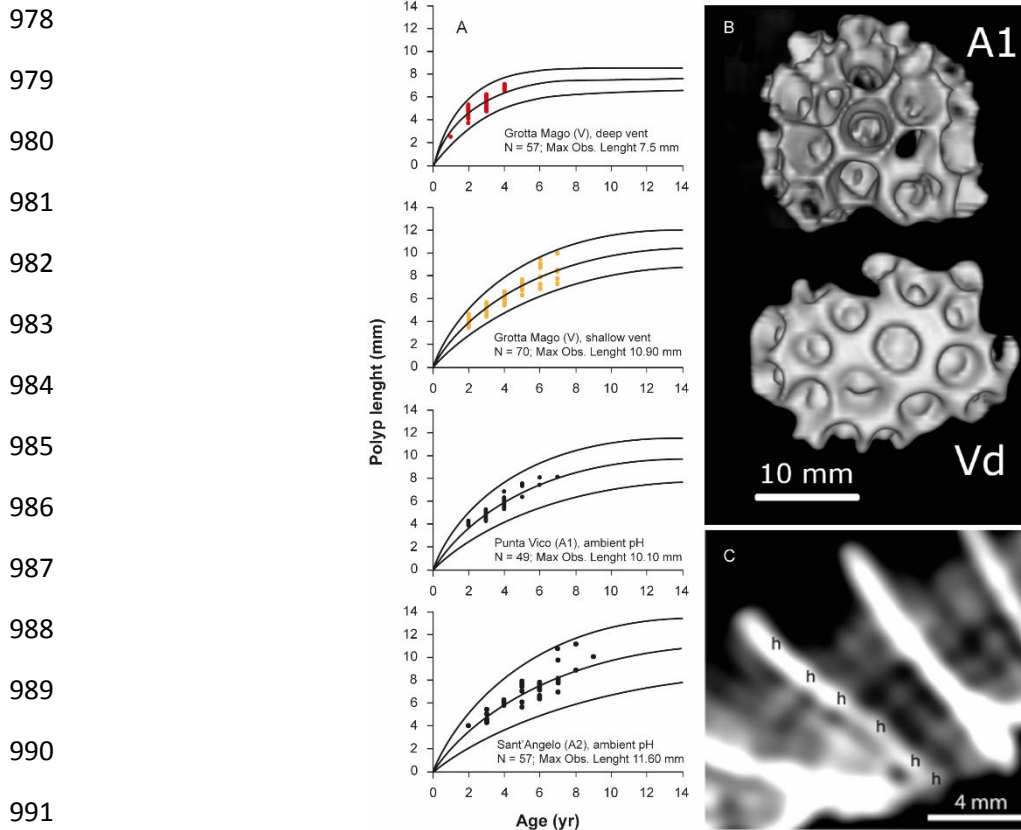
942 **FIGURE 2. A)** Photographs showing colonies sampled for skeletal characteristics and growth of  
 943 the CO<sub>2</sub> vent system and off-vent reference sites with ambient pH. Vent system deep (3 m depth);  
 944 Vent system shallow (1 – 2 m depth), Ambient 1= Punta Vico (1 – 2 m depth); Ambient 2 =  
 945 Sant’Angelo (1 – 2 m depth). Colonies in the vent system exhibited encrusting form (flat growth  
 946 form), whereas colonies in Ambient pH sites were a mixture of massive (extensive vertical and  
 947 lateral growth) and encrusting forms (see also Figure S7). **B)** % Coenosarc (the living tissue  
 948 connecting the polyps) of colonies among the study sites. Significant differences were found  
 949 between vent (shallow and deep) and ambient pH populations ( $F_{3,58} = 24.9$ ,  $p < 0.0001$ ; pair-wise

950 comparisons between vent system deep -shallow and off-vent reference sites  $p < 0.0001$ ). Number  
951 of colonies = 66.

For Review Only



971 **FIGURE 3. Skeletal and growth parameters measured in *A. calycularis*.** A) Skeletal  
 972 parameters of colonies and **B)** Growth parameters at polyp and colony levels at the  $\text{CO}_2$  vent site  
 973 (Vd and Vs) and ambient pH conditions (A1 and A2), respectively. Colony mass and polyp number  
 974 were normalized to colony area. Grey circles in the plot represent the mean. Vd= Vent system  
 975 deep, number of colonies =16; Vs= Vent system shallow, number of colonies = 18; A1= Ambient  
 976 1, number of colonies =17; A2 = Ambient 2, number of colonies = 15. Total number of colonies  
 977 analyzed = 66.



992 **FIGURE 4. Relationships between age-length growth curves of *A. calycularis*.** **A)** Age-length

993 von Bertalanffy growth curves at the polyp (corallite) level. Dots indicate the age determined by

994 counting the growth bands on computerized tomography. Lines indicate the mean von Bertalanffy

995 growth curve and the 95% confidence interval). Values of  $L_{\infty}$  (maximum expected length in the

996 population) and  $K$  (a growth constant, larger for fast growth) were: 7.6 mm and 0.5 for Vent deep;

997 11.0 mm and 0.2 for Vent shallow; 10.2 mm and 0.2 for Ambient 1; and 11.8 mm and 0.17 for

998 Ambient 2, respectively. **B)** Surface 3D rendering of the CT scans performed on a colony of *A.*

999 *calycularis* from Ambient 1 (A1) and on another colony of similar surface area from Vent deep

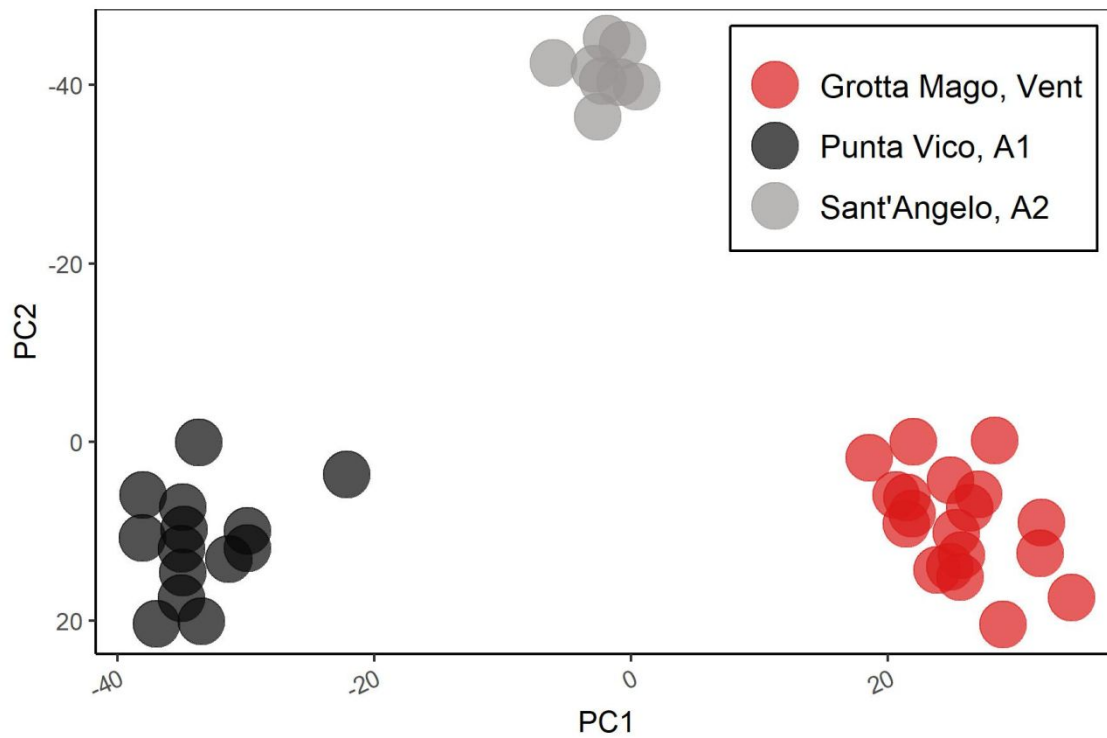
1000 (Vd). Photograph of the deep vent (Vd) colony shows that same calcification is allocated to a minor

1001 number of polyps, and these few polyps result in having a more dense skeleton. **C)** Computerized

1002 tomography scan to count the growth bands on a single corallite. In this photograph, the corallite

1003 of *A. calycularis* is 6 years old; h indicates high density annual bands.

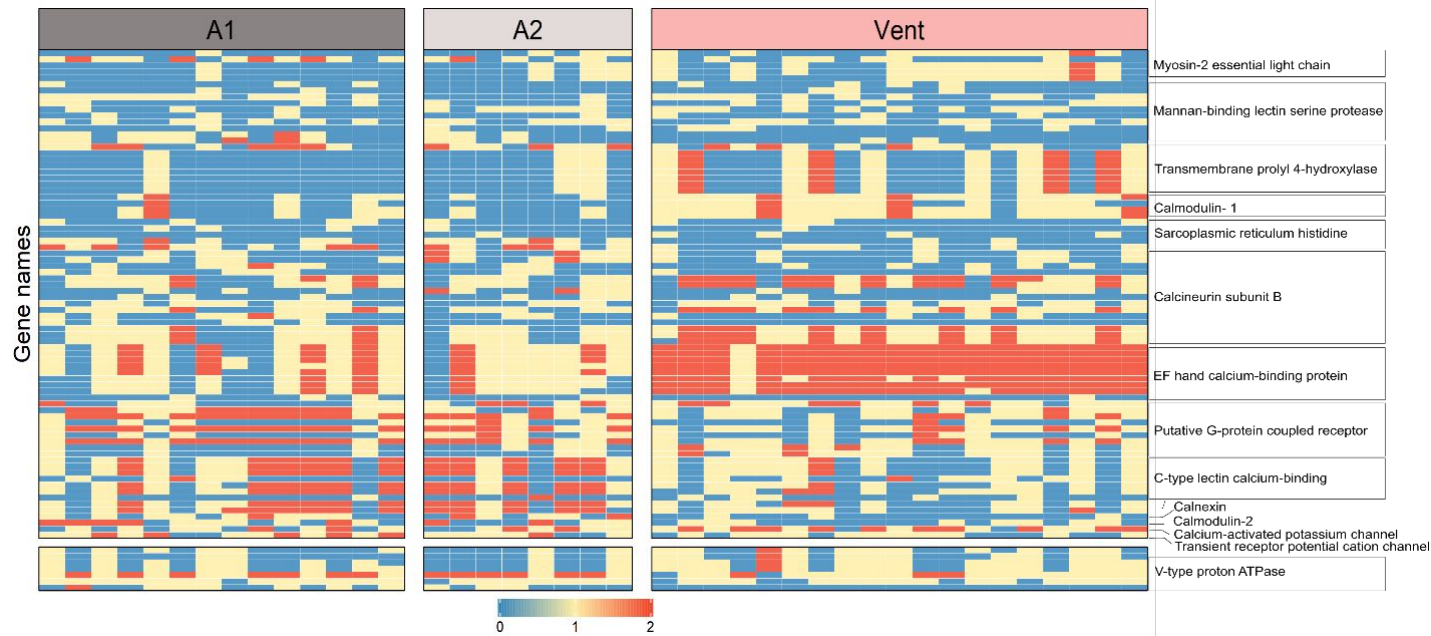
1004



1005

1006 **FIGURE 5. Population genetic structure of *A. calycularis* based on 46,784 single nucleotide**  
1007 **polymorphisms (SNPs).** Number of individuals: CO<sub>2</sub> vent site (Vent, Grotta Mago) = 19; ambient  
1008 pH sites: Ambient 1 (A1, Punta Vico) = 14, Ambient 2 (A2, Sant' Angelo) = 8.

1009



1010

1011

1012 **FIGURE 6.** Upper: SNP genotypes for 13 calcium ion related loci showing high levels of  
 1013 divergence in the Grotta Mago population. Lower: Genotypes for 7 SNPs within a highly  
 1014 differentiated V-type proton ATPase potentially involved in pH regulation in the calcicoblastic  
 1015 layer where calcification occurs. Vent: CO<sub>2</sub> vent (Grotta Mago), A1: Ambient 1 (Punta Vico); A2:  
 1016 Ambient 2 (Sant'Angelo). Legend: 0 = homozygous major allele, 1 = heterozygous; 2 =  
 1017 homozygous minor allele.

1018

1019

1020

1021

1022

1023

1024

1025

1026

1027

1028

1029

1030

1031

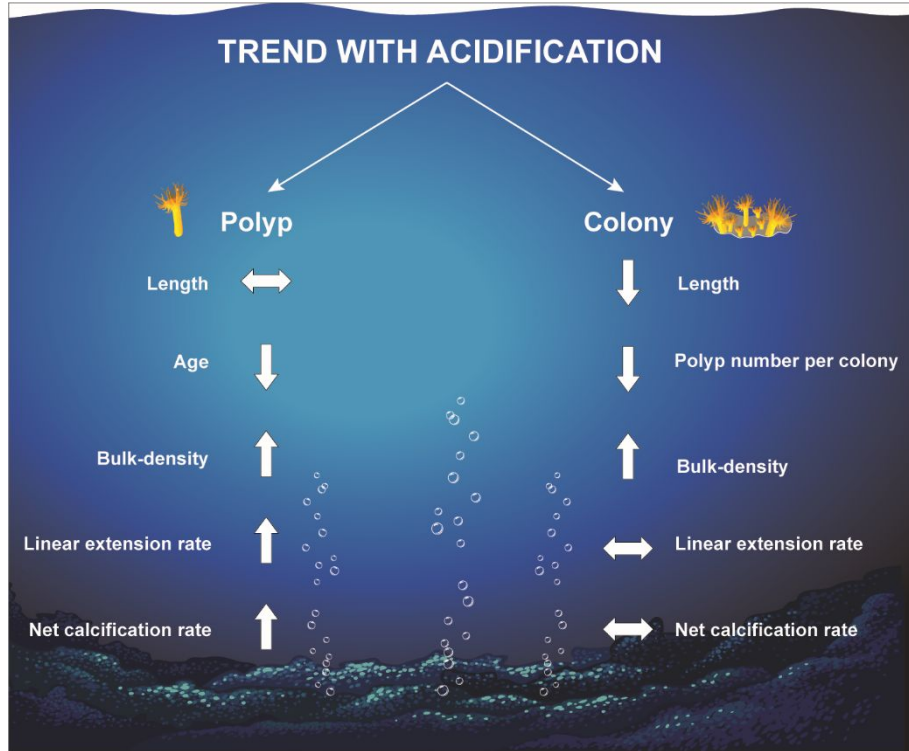
1032

1033

1034

1035 **FIGURE 7. Schematic summary of the responses on skeletal and growth parameters to ocean**1036 **acidification measured in the coral *A. calycularis* at the polyp and colony levels.**

1037



1038 **TABLE 1.** Measured and estimated seawater physiochemical parameters at the CO<sub>2</sub> vent site and  
 1039 reference areas with ambient pH for salinity (S), temperature (T), total alkalinity (A<sub>T</sub>), dissolved  
 1040 inorganic carbon (C<sub>T</sub>), pH<sub>T</sub>, pCO<sub>2</sub>, calcite (Ω<sub>c</sub>) and aragonite(Ω<sub>a</sub>) saturation. Values are means, ±  
 1041 SD with 25th and 75th percentiles. Calculated concentrations of C<sub>T</sub>, pCO<sub>2</sub>, Ω<sub>c</sub> and Ω<sub>a</sub> are shown.  
 1042 1: Parameters measured from discrete water samples; 2: parameters measured with *in situ* sensors.  
 1043 For detailed SeaFET pH sensor statistics and the carbonate system parameters, see Figure S5 and  
 1044 Table S5, respectively.

Month/year	Vent site (GM)			A1-PV	A2-SA
	2m	3 m	4 m	2 m	2 m
<b>September 2018</b>					
S	37.3 <sup>1</sup> ± 0.2 (37.2, 37.5), n=9	37.3 <sup>1</sup> ± 0.2 (37.2, 37.5), n=9	37.3 <sup>1</sup> ± 0.2 (37.2, 37.5), n=9	37.3 <sup>1</sup> ± 0 (37.3, 37.3), n=5	37.4 <sup>1</sup> ± 0 (37.4, 37.4), n=3
T (°C)	25.9 <sup>2</sup> ± 0.2 (25.8, 26.0), n=1530	26.0 <sup>2</sup> ± 0.2 (25.8, 26.0), n=1530	26.0 <sup>2</sup> ± 0.2 (25.9, 26.1), n=1530	17.3 <sup>2</sup> ± 0.4 (17.0, 17.6), n=1331 <sup>2</sup>	25.9 <sup>2</sup> ± 0.2 (59.9, 26.1), n=408
A <sub>T</sub> (μmol kg <sup>-1</sup> )	2564 <sup>1</sup> ± 7 (2561, 2566), n=9	2562 ± 8 (2557, 2565), n=9	2562 <sup>1</sup> ± 8 (2556, 2566), n=9	2618 <sup>1</sup> ± 15 (2607, 2633), n=5	2610 <sup>1</sup> ± 1 (2609, 2611), n=3
C <sub>T</sub> (μmol kg <sup>-1</sup> )	2542 ± 79 (2477, 2585), n=1530	2552 ± 84 (2485, 2593), n=1530	2555 ± 80 (2495, 2598), n=1530	2262 ± 24 (2246, 2276), n=1331	2275 ± 1 (2275, 2276), n=3
pH <sub>T</sub>	7.65 <sup>2</sup> (7.58, 7.90), n=1530	7.62 <sup>2</sup> (7.55, 7.87), n=1530	7.60 <sup>2</sup> (7.53, 7.85), n=1530	8.05 <sup>2</sup> (8.03, 8.07), n=1331	8.02 <sup>1</sup> (8.02, 8.03), n=3
pCO <sub>2</sub> (μatm)	2905 ± 1664 (1724, 3438), n=1530	3146 ± 1928 (1837, 3668), n=1530	3192 ± 1806 (1958, 3799), n=1530	322 ± 34 (298, 341), n=1331	375 ± 1 (374, 375), n=3
Ω <sub>c</sub>	1.68 ± 0.59 (1.21, 2.21), n=1530	1.58 ± 0.56 (1.14, 2.09), n=1530	1.54 ± 0.54 (1.10, 1.98), n=1530	5.96 ± 0.36 (5.74, 6.21), n=1331	5.70 ± 0.01 (5.69, 5.70), n=3
Ω <sub>a</sub>	1.11 ± 0.39 (0.80, 1.47), n=1530	1.05 ± 0.37 (0.75, 1.39), n=1530	1.02 ± 0.36 (0.73, 1.32), n=1530	3.86 ± 0.23 (3.72, 4.02), n=1331	3.71 ± 0.01 (3.70, 3.71), n=3
<b>June 2019</b>					
S	37.8 <sup>1</sup> ± 0 (37.8, 37.8), n=7	37.8 <sup>1</sup> ± 0 (37.8, 37.8), n=7	37.8 <sup>1</sup> ± 0 (37.8, 37.8), n=7	38.0 <sup>1</sup> ± 0 (38.0, 38.0), n=3	37.9 <sup>1</sup> ± 0 (37.9, 37.9), n=7
T (°C)	21.9 <sup>2</sup> ± 2.1 (19.9, 24.1), n=1840	21.8 <sup>2</sup> ± 2.1 (19.8, 23.8), n=1840 <sup>2</sup>	21.7 <sup>2</sup> ± 2.0 (19.6, 23.4), n=1840 <sup>2</sup>	26.2 <sup>2</sup> ± 0.2 (26.1, 26.3), n=408	26.2 <sup>2</sup> ± 1.1 (25.8, 27.0), n=1691 <sup>2</sup>
A <sub>T</sub> (μmol kg <sup>-1</sup> )	2539 <sup>1</sup> ± 22 (2593, 2552), n=7	2541 <sup>1</sup> ± 20 (2532, 2550), n=7	2551 <sup>1</sup> ± 22 (2538, 2568), n=7	2630 <sup>1</sup> ± 1 (2630.1, 2630.9), n=3	2642 <sup>1</sup> ± 17 (2629, 2659), n= 7
C <sub>T</sub> (μmol kg <sup>-1</sup> )	2450 ± 42 (2424, 2464), n=1840	2489 ± 75 (2443, 2509), n=1840	2535 ± 104 (2461, 2574), n=1840	2336 ± 3 (2320, 2353), n=3	2336 ± 23 (2320, 2353), n=1691
pH <sub>T</sub>	7.88 <sup>2</sup> (7.86, 7.98), n=1840	7.74 <sup>2</sup> (7.74, 7.93), n=1840	7.60 <sup>2</sup> (7.56, 7.90), n=1840	8.04 <sup>1</sup> (8.04, 8.04), n=3	7.97 <sup>2</sup> (7.94, 7.99), n=1691
pCO <sub>2</sub> (μatm)	1531 ± 627 (1167, 1653), n=1840	2082 ± 1502 (1352, 2127), n=1840	2812 ± 2310 (1495, 3090), n=1840	372 ± 1 (372, 373), n=3	586 ± 76 (532, 635), n=1691
Ω <sub>c</sub>	2.20 ± 0.41 (2.01, 2.46), n=1840	1.87 ± 0.54 (1.57, 2.26), n=1840	1.60 ± 0.65 (1.10, 2.14), n=1840	5.92 ± 0.01 (5.92, 5.93), n=3	5.34 ± 0.35 (5.08, 5.58), n=1691
Ω <sub>a</sub>	1.44 ± 0.27 (1.32, 1.61), n=1840	1.23 ± 0.35 (1.03, 1.48), n=1840	1.05 ± 0.42 (0.72, 1.40), n=1840	3.89 ± 0.01 (3.86, 3.87), n=3	3.54 ± 0.23 (3.38, 3.71), n=1691

1045

1046